Atmos. Chem. Phys. Discuss., 11, 681–744, 2011
www.atmos-chem-phys-discuss.net/11/681/2011/
doi:10.5194/acpd-11-681-2011

Atmospheric Chemistry and Physics Discussions

Southeast Pacific atmospheric composition and variability sampled along 20° S during VOCALS-REx

G. Allen[1], H. Coe[1], A. Clarke[2], C. Bretherton[3], R. Wood[3], S. J. Abel[4], P. Barrett[4], P. Brown[4], R. George[3], S. Freitag[2], C. McNaughton[2], S. Howell[2], L. Shank[2], V. Kapustin[2], V. Brekhovskikh[2], L. Kleinman[5], Y.-N. Lee[5], S. Springston[5], T. Toniazzo[6], R. Krejci[7], J. Fochesatto[8], G. Shaw[9], P. Krecl[10], B. Brooks[10], G. McKeeking[1], K. N. Bower[1], P. I. Williams[1], J. Crosier[1], I. Crawford[1], P. Connolly[1], D. Covert[3], and A. R. Bandy[11]

[1]Centre for Atmospheric Science, University of Manchester, Manchester, M13 9PL, UK
[2]Dept. of Oceanography, University Hawaii, Honolulu, Hawaii, USA
[3]Dept. of Atmospheric Science, University of Washington, Seattle, Washington, USA
[4]Observation Based Research Division, Met Office, Exeter, UK
[5]Atmospheric Sciences Division, Brookhaven National Laboratory, USA
[6]Dept. of Meteorology, University of Reading, Reading, UK
[7]Dept. of Applied Environmental Science (ITM), Stockholm University, Stockholm, Sweden

[8]Dept. of Atmospheric Sciences, University of Alaska Fairbanks, Fairbanks, AK, USA
[9]Geophysical Institute, University of Alaska Fairbanks, Fairbanks, AK, USA
[10]School of Earth and Environment, University of Leeds, Leeds, UK
[11]Dept. of Chemistry, Drexel University, Philadelphia, PA, USA

Received: 14 December 2010 – Accepted: 16 December 2010 – Published: 10 January 2011

Correspondence to: G. Allen (grant.allen@manchester.ac.uk)

Abstract

The VAMOS Ocean-Climate-Atmosphere-Land Regional Experiment (VOCALS-REx) was conducted from 15 October to 15 November 2008 in the South East Pacific region to investigate interactions between land, sea and atmosphere in this unique tropical eastern ocean environment and to improve the skill of global and regional models in representing the region. This study synthesises selected aircraft, ship and surface site observations from VOCALS-REx to statistically summarise and characterise the atmospheric composition and variability of the Marine Boundary Layer (MBL) and Free Troposphere (FT) along the 20° S parallel between 70° W and 85° W. Significant zonal gradients in mean MBL sub-micron aerosol particle size and composition, carbon monoxide, ozone and sulphur dioxide were seen over the campaign, with a generally more variable and polluted coastal environment and a less variable, more pristine remote maritime regime. Gradients are observed to be associated with strong gradients in cloud droplet number. The FT is often more polluted in terms of trace gases than the MBL in the mean; however increased variability in the FT composition suggests an episodic nature to elevated concentrations. This is consistent with a complex vertical interleaving of airmasses with diverse sources and hence pollutant concentrations as seen by generalised back trajectory analysis, which suggests contributions from both local and long-range sources. Furthermore, back trajectory analysis demonstrates that the observed zonal gradients both in the boundary layer and the free troposphere are characteristic of marked changes in airmass history with distance offshore – coastal boundary layer airmasses having been in recent contact with the local land surface and remote maritime airmasses having resided over ocean for in excess of ten days. Boundary layer composition to the east of 75° W was observed to be dominated by coastal emissions from sources to the west of the Andes, with evidence for diurnal pumping of the Andean boundary layer above the height of the marine capping inversion. The climatology presented here aims to provide a valuable dataset to inform model simulation and future process studies, particularly in the context of aerosol-cloud

interaction and further evaluation of dynamical processes in the SEP region for conditions analogous to those during VOCALS-REx.

1 Introduction

Low-level marine stratocumulus clouds are a persistent feature of the coastal and maritime regions adjacent to continents where cold upwelling water reaches the surface. They play a large role in the climate of these regions (and more widely), yet they are not currently represented well in regional and climate models. Furthermore, many important microphysical processes that control the bulk properties of stratocumulus clouds remain poorly understood.

In 2007, the Intergovernmental Panel on Climate Change (IPCC) Fourth Assessment Report (see Randall et al., 2007; Meehl et al., 2007) identified feedbacks associated with the radiative properties of cloud as one of the major sources of uncertainty in determining how sensitive the global climate system is likely to be to increasing levels of greenhouse gases. Furthermore, the IPCC report also notes that the single largest uncertainty in anthropogenic radiative forcing in the current climate is due to cloud radiative responses to aerosols. Recent studies (e.g., Bony and Dufresne, 2005) have identified tropical boundary layer clouds as the largest contributor to this uncertainty, both in terms of their radiative response (determined by cloud microphysical properties) and in terms of the prevalence of these clouds in particular areas of the world (determined by regional and synoptic meteorology).

Many marine stratocumulus cloud fields are to be found in the subtropics at the eastern edge of the sub-tropical anticyclones, where moisture-rich marine air is cooled by coastal upwelling of cold water from the deep ocean forming semi-permanent cloud decks. The Southern Equatorial Pacific (SEP) region is one the largest regions of stratocumulus clouds (Sc) in the world and is characterized by poorly understood interactions between clouds, aerosols, marine boundary layer (MBL) processes, upper ocean dynamics and thermodynamics, coastal currents and upwelling, large-scale

atmospheric subsidence, and regional diurnal convective circulations. In addition, the great height, steep gradient and extent of the Andes Cordillera acts as a barrier to zonal flow in the South Pacific, resulting in strong winds parallel to the coasts of Chile and Peru (Garreaud et al., 2005). These winds help to drive intense coastal upwelling; and as a result, sea surface temperatures (SSTs) are colder along the Chilean and Peruvian coasts than at similar latitudes elsewhere on the planet. These cold SSTs, in combination with warm and dry air aloft heated by the Andean Altiplano region (plateau) of the Andes (Richter and Mechoso, 2006), combine to support the largest and most persistent subtropical stratocumulus deck in the world. Understanding how these cloud decks are maintained through a balance between radiative cooling, aerosol direct and indirect effects, boundary layer fluxes and entrainment across the strong boundary layer temperature inversion remains an elusive problem. Most climate models still simulate marine stratocumulus cloud fields in the SEP poorly (Ma et al., 1996; Hannay et al., 2009; Wyant et al., 2010), contributing to serious regional SST biases.

As well as the challenging meteorological and dynamical conditions that establish these cloud decks, it is also evident that cloud optical properties over the SEP are strongly linked to atmospheric aerosols (Huneeus et al., 2006), leading to changes in the clouds' radiative properties, influencing their lifetime and behaviour and thereby having a profound effect on the climate system and surface energy budget. Retrievals of cloud droplet effective radii in the SEP derived from satellite observations such as the Moderate Resolution Imaging Spectroradiometer (MODIS) indicate that clouds near to the coast of Chile and Peru are comprised of smaller and thus more numerous) cloud droplets when compared to the pristine marine environment. This scenario of high aerosol concentrations near the coast, declining to pristine conditions to the west (Huneeus et al., 2006; Tomlinson et al., 2007), provides a unique opportunity to observe the effect of aerosol particles on cloud droplet size and reflectance, a problem that is central to the first aerosol indirect effect.

Marine aerosol composition continues to represent a large source of uncertainty in the study of climate and atmospheric chemistry. In addition to their physical size and

chemical composition, hygroscopicity plays a significant role, increasing the particle surface area and radiation scattering potential. The SEP provides an ideal laboratory in which to explore the effects of aerosols on cloud microphysics with contributions from both natural and anthropogenic sources. Extensive mining activities take place along the Andes throughout Peru and Chile, with the emission of considerable amounts of sulphate aerosol. These pollutants perturb the properties of the marine cloud layer and provide a unique, natural laboratory for investigating aerosol-cloud interactions along a strong pollution gradient from east to west, away from the coast.

It is clear therefore that low clouds and the dynamical and microphysical processes controlling the thickness and coverage of marine stratocumulus clouds are a cornerstone of the climate of the SEP; and that the effects of these clouds are not confined to local changes in radiation, heat and moisture budgets. They have profound influences on the regional meteorology and on the ocean currents that feed the equatorial Pacific Ocean and set the environment in which El Niño operates (e.g., Mechoso et al., 1995).

All data used in this study were obtained during the VAMOS (Variability of the American Monsoon Systems) Ocean-Climate-Atmosphere-Land Study (VOCALS-REx; see Wood et al. (2010) for a full overview of the campaign). This campaign, which consisted of a range of aircraft, land and ship platforms, with support from remote sensing instrumentation, intensively sampled the coastal and remote maritime environment between the North Coast of Chile (70.33° W) and 85° W between 19° S and 30° S. Until VOCALS-REx, measurement of cloud properties in the SEP were limited to surface measurements such as those made during scientific cruises transecting the region (Bretherton et al., 2004; Kollias et al., 2004; Serpetzoglou et al., 2008; de Szoeke et al., 2009) and spaceborne remote sensing. Measurement of aerosol and trace gases in the region were hitherto likewise limited to the coastal areas and population centres. The wealth of novel, simultaneous and synergistic measurements of cloud, gas phase and aerosol properties, as well as oceanographic, MBL and free tropospheric thermodynamics, obtained during VOCALS-REx from a range of platforms, will allow the first detailed quantitative investigations of the modulation of marine stratocumulus

cloud properties by aerosol, MBL and surface processes. Furthermore, these data will serve to test and inform regional, climate and cloud-scale modeling parameterizations of this unique environment.

This paper aims to statistically summarise and characterise the mean state and variability of atmospheric composition of the SEP region, above and below the stratocumulus cloud deck – with particular focus on the expected longitudinal gradient in MBL composition from the more polluted coastal zone to the pristine remote SEP. To achieve this, we will use selected data collected onboard three aircraft platforms, a cruise ship and two surface sites below and above the altitude of the synoptic capping inversion (as described in Sect. 2). We will discuss measurements of carbon monoxide, ozone and sulphur dioxide as qualitative tracers of airmass origin, as well as measurements of the abundance, size and chemistry of atmospheric aerosol in the sub-micron diameter size range in the context of their ability to act as cloud condensation nuclei (CCN). These results will be interpreted in conjunction with airmass back trajectories to characterise airmass history. The purpose of such a summary is to provide a set of composition statistics which are relevant to the prevailing meteorological conditions observed during VOCALS-REx and which are also typical of the synoptic conditions of the SEP during Austral Spring more generally. In conjunction with Bretherton et al. (2010), which outlines the thermodynamic and cloud bulk and microphysical variability along 20° S from the same dataset as that used here, these statistics provide a new suite of coordinated measurements of the SEP to serve future chemical and aerosol process studies and modeling activities; and to help relate in situ measurements recorded during VOCALS-REx to remote sensing measurements of cloud and aerosol from space.

2 Data sources

Aircraft platforms used in this study were based at Arica Airport, flying offshore and to the west over the South East Pacific and included the United Kingdom (UK) British

Aerospace-146 (BAe-146), the United States National Science Foundation C-130 (NSF-C130) and the United States Department of Energy Gulfstream-1 (DoE-G1). In addition, we use selected data from the research vessel, Ronald H. Brown (hereafter referred to as RHB), which cruised from the port of Arica and out to 85° S during the period of aircraft operations, as well as spending significant time anchored alongside meteorological buoys at 75° SW and 85° SW. Further details about the VOCALS project and all VOCALS-REx platforms and flight patterns, their configuration and full instrumentation suites can be found in Wood et al. (2010). Aerosol, trace gas and thermodynamic instrumentation for each VOCALS-REx platform appropriate to this study only are listed in Table 2 and will now be described in further detail in this section.

2.1 BAe-146 instrumentation

Instrumentation sampling ambient air inside a converted passenger cabin was fed by a purpose-built stainless steel counter-flow virtual impactor (CVI) or Rosemount cockpit-mounted inlet – the heated CVI was selected for in-cloud sampling with the Rosemount selected in clear air. The transmission of super-micron aerosol particles is reduced to 50% at 2.5 µm diameter due to losses in the flow stream of the inlet with an assumed transmission of 100% for sub-micron particles. Transmission and diffusive losses after the inlet were calculated using aerodynamic theory outlined by Baron et al. (1993), and were found to be negligible across the size range of particles discussed in this work up to the 50% transmission cut-off diameter of the main inlet (2.5 µm). The gas phase instruments were fed from a rearward-facing inlet on the main manifold. Typical air speed and aircraft pitch angle on science runs were around 115 m s^{-1} and +4.5°, respectively.

Thermodynamic, trace gas, aerosol sizing and composition instruments on the BAe-146 and used for this study are listed in Table 2. A GPS-aided Inertial Navigation (GIN) system, consisting of an Applanix POS AV 510 system provided attitude, position and aircraft velocity data. A 5-hole turbulence probe mounted on the aircraft nose was used in conjunction with the GIN system to provide 3-D wind fields and high

frequency (32 Hz) turbulence measurements. GPS position and aircraft orientation were sampled at 50 Hz and recorded at 32 Hz by an Applanix POS AV 510 GPS-aided Inertial Navigation (GIN) unit. Thermodynamic instruments include a General Eastern GE 1011B Chilled Mirror Hygrometer measuring dew-point temperature and a Rosemount/Goodrich type-102 True Air Temperature sensor, which recorded data at 32 Hz using a non De-iced Rosemount 102AL platinum resistance immersion thermometer mounted outside of the boundary layer of the aircraft near the nose. The turbulence probe also used measurements from the GIN and measurements of the ambient air temperature to correct for kinetic effects.

Carbon Monoxide (CO) was measured by an AL5002 Fast CO Monitor, described further by Gerbig et al. (1999); and ozone was recorded by a TECO 49 UV photometer.

Aerosol particle number size distributions were recorded in the nominal range from 10 nm to 3 µm particle diameter. An internally mounted Passive Cavity Aerosol Sizing Probe (PCASP) Type 100 measured ambient particle number concentrations between 100 nm and 10 µm; however only those data between 100 nm and 3 µm are included here due to inlet transmission losses and the focus in this work in the context of CCN which are dominated in terms of number by the sub-micron component. A purpose-built Scanning Mobility Particle Sampler (SMPS), described by Wang et al. (1990), which consisted of a TSI Inc Model 3081 long differential mobility analyser and a TSI inc Model 3786 low pressure water condensation particle counter measured particle diameters between 10 nm to 600 nm. Together, the SMPS and PCASP measure aerosol in a nominal size range of 10 nm to 3 µm diameter.

An optical particle counter (OPC) aerosol instrumentation suite was calibrated at regular intervals prior to and throughout the campaign using calibration latex spheres (refractive index of $1.55+0.00i$) of known diameter. Measured aerosol size spectra were then corrected post-measurement to account for the refractive index of the sampled aerosol. A universal refractive index of $1.4+0.00i$ was assumed for the VOCALS-REx dataset, consistent with an average modeled refractive index derived from the method advised by Tang and Munkelwitz (1996), for an ammonium sulphate and sulphuric acid

mix across the range of sizes and humidities measured during VOCALS-REx by the AMS and thermodynamic instrumentation. No correction from optical particle diameter to mobility diameter was applied to the VOCALS-REx dataset due to the assumed spherical shape of aerosol particles.

Aerosol composition measurements were recorded by a Volatile and Aerosol Concentration and Composition (VACC) system, a Compact Time-Of-Flight Aerodyne Aerosol Mass Spectrometer (AMS) system and a wet nephelometer. The VACC system allows determination of aerosol chemical composition by virtue of functional volatility at characteristic temperatures (see Brooks et al., 2002, for further details). The VACC system comprises a hybrid PMS Optical Particle Counter (OPC), derived from a PCASP, preceded by a 500 W, 20 cm long, 6 mm diameter, tube heater. The aerosol-laden air is continuously sampled through an aspirated Rosemount inlet and a 1 litre plenum chamber and heated to 800 °C in 90 s. The heater temperature is linearly reduced to cabin temperature under computer control. During this thermal cycle (10 min), the hybrid OPC counts and sizes aerosol particles in the diameter range 0.10–3.00 µm. In this study, the maximum particle diameter sized was 0.5 µm due to configuration of the tubing to the OPC in addition to transmission limitations of the Rosemount inlet, which has a 3 µm particle diameter upper limit. The volatility analysis assumes the physico-chemical characteristics of the sampled particles are constant over the scan period (Brooks et al., 2007).

Aerosol Mass Spectrometer (AMS) instruments (described by Jayne et al. (2000) and Drewnick et al. (2005)) use mass spectrometry to determine the chemical functionality of ionized fragments and retrieves the mass loading of the non-refractory, non sea-salt chemical component of sub-micron aerosol, with a 30 s integration time in the case of the BAe-146. The AMS instrument employs thermal desorption, a 70 eV electron ionisation, and an orthogonal extraction reflection time-of-flight mass spectrometer (Tofwerk model C-TOF, Thun, Switzerland). Data were processed and quality assured using the procedures described by Jimenez et al. (2003) and Allan et al. (2003, 2004a), and employed in conjunction with the pressure-dependent calibrations

and corrections described by Crosier et al. (2007), needed for aircraft operation. Mass concentrations are reported for the AMS in the following section for the total organic, sulphate and ammonium components in the aerosol. Nitrate composition is not reported here as concentrations were not recorded above the limit of detection of the instrument (0.05 µg m^{-3}). Component mass size distributions from the AMS could not be derived here with sufficient confidence (signal to noise greater than 1.5) due to the relatively clean environment sampled throughout the majority of VOCALS-REx flights. A collection efficiency of 1 was used for all AMS measurements in this study due to both the acidic nature of the aerosol sampled and the overall low loadings of ammonium aerosol, in-line with recommendations by Matthew et al. (2008), and Crosier et al. (2007).

A wet nephelometer system onboard the BAe-146 comprises two separate instruments operating in series – the first measures sample aerosol in a rycondition. The system does not use an active drying method, rather it relies on inlet ram heating and the increase in temperature in the cabin to reduce the humidity in the sample. This is usually sufficient to obtain "dry" Relative Humidity (RH) values in the range of 20 to 40%. The aerosol sample is then passed through a controlled humidifier, which cycles between a 40 to 90% RH range prior to being sampled by the second instrument in order to measure the scattering coefficient as a function of RH. This allows derivation of the hygroscopic scattering enhancement, f(RH), to be determined.

2.2 NSF-C130 instrumentation

This section discusses selected instrumentation on the NSF-C130 used for subsequent analysis in this study. The aerosol inlet used on the NSF C130 was modeled after the UH inlet described in McNaughton et al. (2007) and the solid diffuser inlet in Huebert et al. (2004). Passing efficiency exceeds 50% for dust particles up to at least 5 µm. Efficiencies for ambient seasalt (i.e., liquid) particles are not well known, but the passing efficiency is sufficient to capture much of the super-µm scattering, so the 50% size cut is >2 µm.

The NSF-C130 aircraft aerosol data discussed here includes measurements of number, size, composition, and optical properties. Total aerosol number concentrations down to 3 nm diameter were measured at 1 Hz with an ultrafine CPC (TSI 3025) and sizes down to 10 nm with two other CPCs (TSI 3010) operated at 40 °C and 350 °C. The CPC at 350 °C reveals the non-volatile number concentration to provide a rapid indication of air mass character also linked to the larger and less volatile sizes commonly effective as CCN in stratus clouds (Clarke and Kapustin, 2010).

Submicron aerosol size distributions between 0.01 and 0.15 mm were measured with an SMPS, described by Zhang et al. (1995) that combined custom electronics with a TSI Model 3081 long differential mobility analyzer and a TSI Model 3010 CPC. Excess air was recycled as sheath air in a closed loop that included a Drierite™ ($CaSO_4$) desiccant that kept relative humidity below 20% so mobility size is regarded here as dry diameter. Both the CPC on the SMPS and another used for monitoring total particle concentrations were operated with the temperature difference increased to 22 °C to achieve a detection limit near 10 nm. Aerosol size distributions were further obtained using a custom laser optical particle counter (OPC, a modified LAS-X, Particle Measurement Systems, Boulder, Colorado). Optically effective size (OES) distributions were obtained between diameters of 0.1 and 10 µm based on spherical calibration particles with a refractive index of 1.588 up to 2 µm and 1.54 above that.

Submicron non-refractory aerosol composition was measured with an Aerodyne Inc. High-Resolution Time-of-flight Aerosol Mass Spectrometer (HR-ToF-AMS, De Carlo et al. 2006) with a nominal 600 °C vaporizer and 70 eV ionizer. To keep flow into the AMS constant, a chamber was mounted immediately upstream of the inlet and maintained at 700 hPa with a pressure controller (Alicat Inc., Tucson AZ) except at altitudes above that pressure, when the chamber was lowered to 300 hPa. The data reported here used V-mode (high sensitivity) and were processed with the procedures of Allan et al. (2003, 2004a) and Aiken et al. (2008). Data with a collection efficiency of unity were used for this analysis for consistency with AMS measurements on other platforms (see Sect. 2.1).

2.3 DoE-G1 instrumentation

The CO concentration was determined by VUV resonance fluorescence using an instrument manufactured by Resonance Ltd., Barrie, ON, Canada. Ozone was measured by a modified UV absorption detector (Model 49–100, Thermo Electron Corporation, Franklin, MA). Measurements of SO_2 from a modified pulsed fluorescence detector (Model 43S, Thermo Electron Corporation, Franklin, MA), were typically below a 200 pptv limit of detection. Further information on gas phase instruments used in VOCALS can be found in Springston et al. (2005) and Kleinman et al. (2007). Two PCASPs, one on a nose pylon and one inside the cabin, measured particles between a nominal size range of 0.1 and 3 µm. Particle size bins were adjusted for a refractive index of 1.41. Deicing heaters were used for both. Size distributions of aerosol particles in the Aitken and accumulation mode were quantified with one-minute time resolution using an SMPS (scanning mobility particle sizer) consisting of a cylindrical differential mobility analyzer (DMA) and a condensation particle counter. It is assumed that particles are spherical so that mobility and geometric diameters are equal. Data were analyzed using the inversion algorithms described by Collins et al. (2002). A Nafion dryer upwind of the DMA reduced relative humidity to 14% (1σ=2%). A global normalization procedure to match SMPS and PCASP number concentration, especially at the low end of the overlap region where the PCASP efficiency decreases is described by Kleinman (2010).

2.4 Surface site instrumentation

Surface aerosol measurements were carried out at the European Southern Observatory at Paranal (2635 m a.m.s.l., 24.75° S, 70.4° W), 150 km south of Antofogasta in Northern Chile; and at Paposo (690 m a.m.s.l.), located to the south of the 20° S study region at 25.04° S, 70.45° W. Instrumentation was installed on the windward edge of the top of the mountain telescope platform, free from local pollution and perturbations. Sample air was brought to the instrumentation via 1/4″ stainless-steel inlet.

Total aerosol number concentration greater than 10 nm diameter was measured using a condensation particle counter (CPC) model TSI 3010. The aerosol size distribution between 10 and 400 nm was measured with a closed-loop sheath air Differential Mobility Particle Sizer (DMPS) operated in stepwise mode utilising 15 bins, with a 20 s integration time for each bin, thus recording a size distribution every 300 s. Counting-statistics uncertainties are smaller than 5%. The aerosol size distribution between 260 and 2200 nm was observed with an optical particle counter (OPC) GRIMM, model 3.709, which sized the particles in 12 bins at 1 Hz, recording 1-min averages. For a composite aerosol size distribution covering size range from 17 to 2200 nm, OPC data were averaged and merged with the DMPS-derived size distribution. The first bin of the OPC data was removed due to problems with instrumental electronic noise.

2.5 Cruise ship instrumentation

On the RHB, submicron particles were sampled through an isokinetic inlet located above the laboratory containers on the forward deck of the ship and approximately 18 m a.s.l. and delivered to the containers and instruments therein (Bates et al., 2008). An Aerodyne Quadrupole Aerosol Mass Spectrometer (Q-AMS) measured bulk, non-refractory submicron aerosol chemical composition and component-specific size distributions in real time. Quantified chemical components included sulphate, nitrate, ammonium and organic mass. Concurrently, particulate samples were collected by multistage impactors; these were analyzed for sulphate and ammonium by ion chromatography and for organic mass by Fourier transform infrared spectroscopy and were used to establish the collection efficiency of the Q-AMS.

2.6 Data quality

Extensive pre-campaign and pre-flight calibrations and tests were carried out on all platforms to ensure optimal instrument performance, including, a dedicated test flights to examine and rectify potential problems before scientific measurement. The quality of

the dataset used here has also been tested rigorously in the post-campaign period by comparing data between similar instruments operated both on the same platform and across platforms to ensure consistency. The nature of such tests was three-fold: firstly, where available, common instrumentation was compared for each platform to ensure internal consistency; secondly, instruments on different aircraft were compared for six 10-min trailing intercomparison straight and level runs made by each aircraft below, in and above cloud level on two occasions during the campaign; and thirdly, the data were compared statistically over the whole campaign in common locations to examine any potential systematic biases between the instruments. Further details of the dedicated aircraft intercomparison exercise can be found in Table 11 of Wood et al. (2010).

2.6.1 Thermodynamic data quality

Thermodynamic and wind measurements from equivalent instruments (see Table 2) were compared between the NSF-C130, DoE-G1 and BAe-146 aircraft for 10-min trailing intercomparison runs. Mean quantities were found to agree within 0.1 K, 0.3 hPa and 0.2 m s^{-1} on average in the case of temperature, pressure and horizontal wind velocity, respectively; and in all cases, agree well within the sampling variability (sampled means for each instrument are all within 1-standard-deviation of sampled atmospheric variability).

2.6.2 Trace gas data quality

Mean concentrations of carbon monoxide and ozone were calculated for trailing intercomparison 10-min runs and were found to differ by less than 1.5 ppbv between the three aircraft, which is well within the quoted precision of the instruments and also within one standard deviation (5 ppbv) of the total sample mean for each intercomparison run. Therefore we quote an upper limit of 1.5 ppbv as the uncertainty on the CO data used in this study. An equivalent comparison for ozone showed maximum differences to be less than 4 ppbv.

2.6.3 Aerosol data quality and interpretation

The multiplicity of aerosol sizing spectrometer instruments both on each platform and between platforms in VOCALS-REx allows good confidence in the accuracy of quantitative data and the statistical significance of the sampling.

Aerosol sizing instruments were validated by comparing the integrated aerosol volume in mutually overlapping size measurement channels as measured by different instruments. A similar analysis for equivalent instruments listed in Table 2 was performed for all platforms.

Aerosol spectra from each instrument were corrected to dry size using the derived sample relative humidity recorded near the sample point of each instrument together with modeled aerosol growth factors calculated for ammonium bisulphate with organics in proportions indicated by AMS measurements using the Aerosol Diameter Dependent Equilibrium Model (ADDEM) described by Topping et al. (2005). This model uses a thermodynamic modeling framework to predict the equilibrium behaviour of multi-component aerosols, coupled with a technique for finding a solution to the Kohler equation in order to create a diameter dependent hygroscopic aerosol growth factor. Correcting all size spectra to their equivalent dry size in this manner allows direct intercomparison of measurements and also facilitates the subsequent calculation of cloud droplet activation and growth under varying ambient conditions.

Following the above correction, aerosol size spectra were intercompared to check for consistency. The integrated volume of aerosol measured between 10 nm and 700 nm is comparable to the measured AMS particulate, assuming a density of 1.65 g cm^{-3}. Average ratios of this aerosol size spectrum integrated volume to the AMS-derived volume were in the range 1.1 to 1.5, lending confidence to the data. The reason for the positive bias is most likely due to the insensitivity of the AMS to refractory aerosol such as sea salt which is expected in this marine environment.

Data from all aerosol spectrometer instruments were also compared between platforms during dedicated intercomparison trailing runs as described earlier, to look for

systematic bias and to understand sampling variability. No significant systematic biases between the four aircraft were observed and independent mean quantities over each intercomparison run were all within one standard deviation of the total sample and therefore indistinguishable from the sampled variability.

3 Data sampling

A 20° S flight pattern, discussed further in Wood et al. (2010) was designed to create a vertical cross-section of the boundary layer, cloud and lower free-tropospheric structure. It included a sequence of above-cloud legs at 100–300 m above the capping inversion, in-cloud legs flown near the middle of the stratocumulus layer (or slightly under the inversion in the absence of stratocumulus), and sub-cloud legs flown at various levels between 40 and 60 km long, typically interspersed with a deep profile to 3 km altitude after every other repetition of the leg. Each mission began with a take-off from Arica Airport and a transit at low altitude to a point at 72° W, 20° S (designated Point Alpha) before beginning the above sequence whilst flying due west along 20° S for as far as aircraft endurance allows. In the case of the NSF-C130, such endurance was typically around 9 h allowing sampling to 86° W, reducing to 80° W for the 5-h endurance of the BAe-146, and 78° W for the 4-h endurance of the DoE-G1.

VOCALS-REx flights used in this analysis are listed in Table 1 with flight tracks from the corresponding flights for each platform plotted in Fig. 1, showing a vertical-longitudinal cross-section curtain of flight tracks for each platform along the 20° S parallel. Four NSF-C130 flights (RF03, 04, 05, 10) and six BAe-146 flights (B408, 410, 412, 414, 417, 420) were fully dedicated to the 20° S pattern. In addition, the 20° S pattern was flown on portions of other flights on transits to or back from different mission types, e.g. intercomparison over-flights of the RHB. The four dedicated NSF-C130 20° S flights sampled from 06:00–15:00 UTC; in the sampling region, sunrise was around 11:00 UTC so the outbound legs were entirely nocturnal, while the return legs sampled the initial morning evolution of the boundary layer. The NSF-C130 flights

RF02,13 and 14 sampled along 20° S from 13:00 to 16:00 UTC. The BAe-146 flights typically spanned the range 08:30–12:30 UTC. In total, over 140 h of flight sampling time are considered in this study.

Due to the nature of the flights, the near-coast MBL environment (east of 75° W) at 20° S was extensively sampled as shown in Fig. 1, during both the pre-dawn and late morning. Further offshore the sampling was weighted to around 12:00 UTC (post-dawn), with three flights providing midday coverage. Sampling of the free troposphere was less prescriptive than that of the MBL and consisted of several saw-tooth profiles during the 20° S pattern in addition to climbs and descents made between the MBL and high level transit altitudes.

In summary, the range of 20° S flights conducted during the campaign are weighted toward greater sampling of the MBL with a generally reducing sample time with distance offshore due to the differing endurance of the three aircraft.

3.1 Data statistics

To provide a statistical summary that is concomitant with thermodynamic properties discussed by Bretherton et al. (2010), we extract only those data recorded within 1-degree of latitude north and south of the 20° S parallel for a period between 16 October 2008 and 15 November 2008. The statistical dataset of atmospheric composition presented in the following section was carefully merged to provide consistently sampled data from all platforms. To represent the MBL to this end, only those data obtained at less than 1200 m altitude or below cloud (whichever was lower) were used, to ensure data were not subject to potential artefacts of cloud-contamination such as droplet shattering and that all data were below the altitude of the capping inversion, which was observed not to exceed this altitude. Data were screened for the presence of cloud, using a threshold in measured liquid water content (LWC) of 0.05 g kg^{-1} and were further screened for drizzle using a cut-off threshold of 5 droplets cm^{-3} as measured at sizes greater than 30 µm. For the BAe-146 and NSF-C130, LWC was calculated from data recorded by a Droplet Measurement Technologies (DMT) Cloud Droplet Probe

(CDP) and from a DMT Cloud Aerosol Particle Spectrometer (CAPS) in the case of the DoE-G1. Similarly, to represent a free tropospheric layer close to cloud-top (hereafter referred to as the FT), only those data between 1700 m and 3200 m were extracted and the same cloud-screening test applied, though no clouds were flagged in this vertical layer.

All data were then gridded into seven bins of 2.5-degree longitude width between 68.75° W and 86.25° W. For each of these bins, a set of mean, median, upper and lower quartile and decile values were calculated for each variable. Gridded data were then weighted according to their total sampling time and merged with data from other platforms to provide a dataset representative of the mean state and natural variability sampled by all platforms along the 20° S parallel.

4 Results

In this section we investigate the airmass history of air sampled along 20° S both in the FT and in the MBL before interpreting the measured composition in this context.

4.1 Meteorology and dynamics

The SEP region is dynamically complex, particularly in the near-coastal area where turbulent processes such as diurnal pumping of the High Andes surface layer are coupled to synoptic-scale coastal dynamics (e.g., Rahn and Garreaud, 2010b). This results in frequent outflow of continental PBL air directly into the FT. Furthermore, the MBL is dynamically linked to the FT through entrainment of subsiding air in the sub-tropical anticyclone.

The variable character of the synoptic meteorology during the VOCALS-REx campaign as described by Rahn and Garreaud (2010a,b); Toniazzo et al. (2010) implies a potentially different origin, on average, for the air-masses in the area of observation before and after the beginning of November. Between 15 October 2008 and 31 October

2008 elevated baroclinic wave activity in the subtropical jet stream (STJ) was concomitant with a high surface pressure anomaly over much of the domain between 90° W to 70° W, 40° S to 10° S. In the boundary layer, the flow was south-easterly near the coast, veering easterly offshore, as is typical of the regional climatology. In contrast, between 2 November 2008 and 17 November 2008, a more quiescent STJ was observed aloft, with boundary layer circulation remaining typical of the regional climatology, but offshore the winds were more southerly than in late October 2008, indicating a longer marine residence time and reduced transport of polluted coastal air offshore at 20° S. Air-mass subsidence in the FT over the region is fairly steady and diabatic in nature, with a larger contribution from tropical (and possibly continental) origins compared to late October 2008.

To better understand this potential difference in airmass origin and hence pollution sources, 10-day back trajectories were calculated daily in both the FT and the MBL. For back trajectory analysis, the MBL and FT must be treated separately and with different methods. In the FT, subsiding air and a strong temperature inversion at the top of the MBL, which strongly inhibits convection, gives confidence in the use of back trajectories which employ vertical advection, allowing the investigation of long-range and long-term airmass history. Conversely in the MBL, entrainment processes across the temperature inversion, inherent turbulent motion and surface effects are not represented in current Lagrangian trajectory models which model vertical motion and which use operational reanalysis vertical wind fields. For these reasons, we model 10-day vertically dynamic back trajectories for the FT but use 5-day isobaric trajectories in the MBL. Trajectories for the FT presented here were driven using 3-D thermodynamic fields produced by the European Centre for Medium Range Weather Forecasting (ECMWF) operational analysis Integrated Forecasting System (IFS Cycle 29r2) on a 1.125×1.125 geospatial grid on 91 hybrid model levels. We choose these time constraints to limit the uncertainty in airmass origin beyond these times as assessed by ensemble analyses – trajectories typically diverge by more than two degrees of latitude or longitude beyond these times with model level perturbations in trajectory endpoint thermodynamic properties.

Furthermore, the choice of isobaric transport in the MBL allows qualitative determination of mean airmass advection in the mean MBL flow. Comparison of ECMWF and NCEP reanalysis wind fields with horizontal winds measured by the NSF-C130 and BAe-146 and presented in Bretherton et al. (2010), show excellent agreement and confidence in the use of such trajectories in the MBL.

However, in choosing these different trajectory methods for each atmospheric layer we must note that entrainment and diabatic processes can be discussed only qualitatively. A process study of such entrainment processes and their impacts on the climate of the SEP will be discussed in forthcoming work by Clarke and Kapustin (2010).

Figure 2 shows a sample of free tropospheric 10-day back trajectories initiated at half-degree intervals of longitude along 20° S between 70.5° W and 90° W for two sample days. This sample illustrates the typical and general synoptic flow regime observed in all trajectories within each of the two meteorological periods identified above. In general, we observe that FT air sampled along 20° S always originates in the Southern Hemisphere, with coastal airmasses, seen as redder shades to the east of 74° W in the left panels of Fig. 2, having been advected long-range and eastward across the Pacific in the southern STJ within the previous few days before rapidly descending near the coast of South America and advecting northward near and parallel to the Chilean coastline. Such descent is further illustrated in the right panels of Fig. 2 which show yellow and red colouring at atmospheric pressures consistent with residence below cloud-base. On 18 October 2008 (top panels of the figure), we see that air arriving at 20° S is always subject to recent rapid descent and and generally from the east with the exception of coastal trajectories to the east of 74° W, which show advection along the Chilean coast at low level (below 900 hPa) over the previous 3 days. Further offshore, between 74° W and 80° W, we see trajectories that also reflect long-range eastward transport in the STJ followed by descent and advection parallel to the coastline. However, these trajectories remain more than 200 km offshore. In contrast, airmasses in the remote SEP (west of 80° W) do not show any contact with the coast and instead descend along an eastward trajectory. On 6 November 2008 (bottom panels of the figure), as for 18

October, we see the same broad airmass origins to the west of 74° W, yet in contrast to 18 October 2008, coastal trajectories (east of 74° W) display advection near the surface but along the Peruvian coast to the north. In summary, this sample of FT trajectories demonstrates a variable and complex vertical interleaving of airmasses from diverse sources, with long-range upper tropospheric transport from the east dominating to the west of 74° W, yet with both long-range transport and lower level advection from South American coastal regions to the north and south of 20° S nearer to the coast. This suggests local and more variable coastally dominated pollutant sources for FT airmasses to the east of 74° W and more diverse pollutants from a variety of long-range sources to the west of 74° W.

In contrast to the FT, Fig. 3 shows isobaric trajectories initiated daily at 950 hPa, representing mean MBL flow within each period. Daily trajectories are initiated at 72° W, 76° W and 85° W to illustrate the divergence of airmass origin with distance offshore. The MBL trajectories display no significant difference across the period of VOCALS-REx and display the same overall pattern in terms of continental influences. Coastal zone trajectories (those initiated at 72° W) all pass over the continent, terminating on contact with the terrain. Those initiated further offshore demonstrate that land contact is made only in some trajectories, whilst those in the remote zone have not passed over land in the past five days at least. The similarity in MBL flow across the campaign seen in Fig. 3 suggests that variability in MBL composition is influenced less by the small variability in the direction of MBL flow and more by variability in the emissions of point sources (e.g., cities and industrial plants) common to all periods as well as the higher evident variability of FT airmasses and the potential entrainment of episodically polluted air into the MBL from above, as will be discussed by Clarke and Kapustin (2010).

To distinguish between these broad airmass history regimes with distance offshore in the following analysis, we define three longitudinal zones: a coastal zone (70° W to 75° W); a transition zone (75° W to 80° W); and a remote zone (80° W to 85° W). We shall use these zones to distinguish composition properties in the following discussion.

4.2 CO, O_3 and SO_2

In conjunction with other pollutants, CO can also be used to differentiate airmass origin and as an indicator of typical background states for the SEP environment. Ozone, unlike CO, is a relatively short-lived (1 week) species, with production and loss rates being highly dependent on the local chemical environment. Carbon monoxide is a relatively long-lived (2 months in the troposphere) tracer of many land-based combustion sources (e.g., Staudt et al., 2001). It is a predominant combustion marker of both fresh and aged biomass burning and urban plumes and is typically well-correlated with aerosol number concentration due to their often mutual combustion sources (e.g., Allen et al., 2007). In conjunction with ozone concentration and aerosol composition such as that afforded here, CO can also be used to differentiate source-type and relative age of polluted airmasses. Sulphur dioxide is a product of oxidation of many forms of atmospheric sulphur, both biogenic and anthropogenic. Sources of sulphur in the SEP region are many, with volcanic activity in the Andes leading to a direct injection of SO_2 into the free troposphere (Loyola et al., 2008), as well as strong emissions from extensive smelting industry throughout Chile and Peru (Carn et al., 2007). Biogenic sources include the ozone-mediated oxidation of dimethyl sulphide emitted from the sea-surface layer (e.g., Norman and Wadleigh, 2007).

Longitudinally-gridded concentration statistics derived as described in Sect. 3 for carbon monoxide, ozone and sulphur dioxide in the MBL and FT along 20° S are plotted in Fig. 4, with sampling times and diagnostics given above each longitude grid. Figure 4 shows a clear longitudinal gradient in mean CO concentration in the MBL, decreasing with distance from the South American Coast. The highest mean concentrations of CO in the MBL were seen to be 74 ppbv at 70° W with upper and lower deciles extending to 80 ppbv and 68 ppbv, respectively and an inter-quartile range of 6.4 ppbv. The inter-quartile range is similar to the difference between the quartiles and deciles, with near equal median and mean concentrations, reflecting a near Gaussian distribution of CO concentration in the MBL. To the west of 76° W, CO falls to a near constant mean

background of 63 ppbv and associated variability in this more remote marine environment is also reduced with an inter-decile range of 4 ppbv and and inter-quartile range of 2 ppbv at 84° W, although we must note the reduced sampling time (1 h) of the remotest zone compared with the near-coast (up to 19 h). In the transition zone between 75° W and 80° W we observe a shallower gradient in the mean CO concentration and variability between the more variable coast and more constrained remote SEP, with inter-decile range of between 6 ppbv and 10 ppbv.

In contrast to the MBL, the story in the FT is very different: mean CO concentrations are significantly higher at between 70 and 80 ppbv at all longitudes. Also, variability is much higher, with inter-decile ranges of up to 28 ppbv and inter-quartile ranges in excess of 10 ppbv. There is evidence for a decreasing gradient from the coast out to the edge of the transition zone, followed by a slight elevation to the west of 80° W, though we must again note the poor sampling in the remote FT zone (1.3 h over 2 flights). The higher mean concentration and variability in the FT compared to the MBL supports the general back trajectory analysis that the FT is highly variable in terms of airmass origin and may frequently carry CO from long-range sources in Australasia. From the MBL gradient in CO concentration, it is possible to conclude that the coastal zone is characterised by dynamical contact with the continent and its combustion sources as suggested from trajectory analysis. Similarly, the greater variability in CO in the MBL near the coast is expected to reflect the variability in the emission strength of such sources. The more constant remote concentrations indicate the absence of sources and defines a consistent marine background concentration for the VOCALS-REx campaign.

Ozone (see Fig. 4) concentrations were consistently very low in the MBL at around 27±5 ppbv in comparison to northern hemispheric background concentrations (e.g., 64 ppbv in the Central US, Lefohn et al., 2001) and of similar concentration to other southern hemispheric MBL environments (e.g., 20 to 25 ppbv in the Tropical Western Pacific reported by Allen et al., 2007). There is evidence for a trend toward marginally lower background ozone concentration in the near-coast (around 20±5 ppbv at 70° W).

In the FT, ozone is significantly higher and more variable on average, with concentrations in excess of 60 ppbv in the remote zone. Also, the trend toward lower ozone concentrations in the near-shore is much more pronounced than in the MBL, with mean concentrations falling to 35 ppbv. However, ozone is at all times observed to be elevated above cloud top compared with below, which may be explained to some extent by the predominating descent of airmasses from the ozone-rich upper troposphere. There is some evidence to suggest an anti-correlation between ozone and CO, especially in the coastal zone which may indicate relatively fresh combustion sources and a net destruction of tropospheric ozone, yet such a relationship must be examined with the above potential dynamical explanation in mind.

Sulphur dioxide has its own unique story, with evidence for much more frequent pollution episodes. Mean boundary layer concentrations are between 20–30 pptv at all longitudes, but there are clear extremes in the deciles near the coast, extending up to 140 pptv. Medians are negatively skewed with respect to mean concentrations suggesting a non-gaussian concentration distribution with occasional episodes of high concentrations. In the free troposphere, sulphur dioxide concentrations in the remote zone are similar to those in the MBL, however the coastal FT environment is observed to be more frequently polluted.

To further characterise the relevance of these pollution episodes, we present probability density functions of gas concentrations in Fig. 5. Gas concentrations are gridded for frequency analysis into 2 ppbv, 4 ppbv and 5 ppbv bins for CO, O_3 and SO_2, respectively and divided into 5-degree longitude zones representing the coast, transition and remote regions as described earlier and further sub-divided into MBL and FT components. Total sampling times are included in each panel of Fig. 5. In the case of CO in the MBL (Fig. 5a), we see a long tail in the distribution extending up to 100 ppbv, which is absent in the transition and remote zones. In the FT (Fig. 5b), a long tail in the CO distribution is noted in all zones, however we note an apparent bi-modality in the coastal zone with peaks at 58 ppbv and 80 ppbv. The long tail feature seen in CO in the MBL near the coast is consistent with dynamical contact with continental combustion

sources. Ozone PDFs in the MBL show little longitudinal structure, as noted in Fig. 4, with a peak MBL background of between 25–30 ppbv. However, there is evidence for structure in FT ozone, with modal peaks at 24 and 34 ppbv near the coast and peaks only at 34 ppbv in the transition and remote regions. This could suggest that we are observing uplift of MBL ozone-poor air (which is typically lower in concentration) into the FT near the coast, which is consistent with the hypothesis of up-slope pumping and outflow above cloud top. This is further supported by examining the correlation between ozone and specific humidity – high specific humidity being a very reliable tracer of MBL airmass in this region of synoptically descending dry air. Figure 6 shows a scatter plot of aircraft leg-averaged ozone concentration versus specific humidity, colour-coded for longitude and symbolized for above or below-cloud sampling. From the figure it is clear to see that elevated ozone concentrations are typically associated with low specific humidity and vice versa. This would suggest that ozone-rich air is indeed sampled in the background dry descending air in the FT, with high ozone being transported down from the ozone-rich upper tropical tropopause layer. And conversely, ozone-poor air appears to be relatively moisture-rich and therefore likely uplifted MBL air onshore. Measurements in the transition region (blue symbols) also appear to represent a mixing line between these two extremes. Further quantitative examination of such mixing is hindered by the non-conservative nature of ozone chemistry, especially in the boundary layer where deposition to the surface dominates. The sulphur dioxide PDF in the MBL displays a long tailed distribution to high concentrations with a mode at 15 pptv. This long tail is absent in the corresponding FT PDF which has similar mode at 15 pptv, yet little continuity between this mode and the very high concentrations represented by the right-hand axis of the PDF which shows an increased frequency (15% to 20%) of very highly elevated SO_2 episodes in the FT compared to the MBL (5% to 8%). This long-tail in the SO_2 distribution in the MBL is suggestive of dynamical mixing with the FT. The elevated SO_2 events in the FT, observed as discrete layers may be linked to smelting activity in the area; very high outflow of sulphur dioxide and heavy metals from smelters in both Chile and Peru has been well-documented (e.g., Romo-Krögera

et al., 1994). The outflow of anthropogenic sulphur from northern Chile has also been linked to impacts on the offshore stratocumulus cloud deck (Huneeus et al., 2006).

In summary, there is a gradient in the MBL with distance offshore; and variability in all MBL tracers is enhanced in the coastal region. The FT is much more complex and variable and displays a vertical interleaving of airmasses of very different origins, CO, ozone and SO_2 are all elevated in the mean in the FT relative to the MBL, yet the nature of such elevations is noted to be highly episodic, with the frequency of these pollution episodes increasing in the coastal region. As well as the potential influence of long-range transport, there is evidence, in terms of ozone and water vapour, for pumping of coastal MBL air into the FT up the slopes of the Andes and also for the reverse exchange with long tails in CO and SO_2 seen in the MBL near to shore. Such processes will be discussed further by Clarke and Kapustin (2010).

4.3 Aerosol composition

We consider only the sub-micron aerosol component here, which dominates the number concentration of particles and the activated fraction in terms of CCN activity; with number, as well as chemistry, being important in terms of CCN activity. Whilst super-micron particles have large individual mass, such particles are less in number and therefore do not contribute significantly to CCN activity, although we note the potential role of Giant CCN (>5 µm diameter) in stratocumulus radiative and precipitative properties (Feingold et al., 1999). The implications of GCCN for marine stratocumulus in VOCALS-REx is beyond the scope of this study.

Longitudinally-gridded aerosol mass concentration statistics along 20° S of non-refractory sub-micron diameter sulphate, organic and ammonium components measured by AMS instruments on aircraft and RHB platforms are plotted separately for the MBL and FT in Fig. 7. Mean data from the RHB are plotted in each longitude bin as purple circles in the MBL (left panels), along with quartiles and deciles (as purple bars) for periods when anchored on station at 75° W and 85° W over several days in late October. The RHB sea-surface results are consistent with the variability in mass concentrations

sampled by the aircraft demonstrating that the surface sub-micron aerosol composition is representative of the mean MBL state as expected due to turbulent mixing of sub-micron aerosol.

Comparing zonal structure in aerosol composition in Fig. 7 with that of CO in Fig. 4, we see a clear correlation with distance offshore, with decreasing loadings of all aerosol components as well as the same increased variability near to shore. The gradient in ammonium and sulphate is more evident than for organics with mean sulphate loadings of 2 µg m^{-3} at 71° W reducing to <0.5 µg m^{-3} at 84° W and ammonium reducing from 0.25 µg m^{-3} to <0.1 µg m^{-3} over the same range. This perhaps suggests a common source for CO, sulphate and ammonium aerosol in the coastal region. Again, the FT displays a different character, with much reduced concentrations of sulphate and ammonium but near equal levels of organics, with a peak in FT organics at 80° W, characterised by episodic events seen as a wide 90th percentile whisker. This increase in organics in the remote zone is simultaneous with increased CO in the FT and therefore suggests that the elevated organics sampled there have been carried with the CO in long-range transported plumes from Australasia, perhaps in aged biomass burning plumes such as those documented in Heyes et al. (2009).

The dominance of the sulphate mass fraction over other aerosol components measured by the AMS is typical of southern hemispheric marine locations (e.g., Allen et al., 2007). Mean loadings observed during VOCALS-REx in the remote zone are typically less than 0.3 µg m^{-3}, which is similar to measurements recorded in other southern hemispheric marine studies, such as those recorded in the South Atlantic by Zorn et al. (2008), reporting a marine sulphate background of around 0.3 µg m^{-3}. Such loadings are very low relative to marine airmasses in the Northern Hemisphere for example, with typical Eastern Atlantic loadings of 5 µg m^{-3} measured during the Reactive Halogens in the Marine Boundary Layer (RHAMBLE) experiment (Allan et al., 2009). Organic and ammonium loadings are also very low by Northern Hemispheric and continental averages.

This low mean sulphate and ammonium concentration in the remote MBL suggests a predominantly marine source for the residual loadings, with sulphate aerosol in the remote zone expected to be produced as a result of the oxidation products of dimethyl sulphide (DMS), and methyl sulphonic acid (MSA, Ayers et al., 1991; Mari et al., 1998) as well as the direct oxidation of SO_2 in cloud droplets. As well as sulphate, we also see that around 20% of the mass measured by the AMS is of an organic nature. MBL aerosol particles have often been found to contain significant amounts of organic matter (Novakov et al., 1993). This fraction has been linked to biological activity in the ocean (Novakov, 1997; O'Dowd et al., 2004), although the ubiquity, precise formation mechanism, chemical nature and importance of this fraction currently remain the subject of debate (Allan et al., 2008; Facchini et al., 2008). As well as the natural particulates, there is also a contribution to the organic fraction from shipping and long-range transport of terrestrial emissions (Raes et al., 2000). However we do not rule out the importance of entrainment of elevated organics from the FT into the MBL, which may be the cause of increased organic variability in the remote zone. Correlation between sulphate and CO near to shore (east of 73° W) suggests a predominantly continental origin.

Aerosol mass spectra (not shown here) show typical peaks associated with sulphate aerosol at *m/z* 18, 32, 48, 64, and 80 with peaks from ammonium at 15, 16 and 17. There is no evidence of significantly different organic functionality between the two zones, however a prominent organic peak at *m/z* 44 represents CO_2^+, which arises from carbon dioxide due to the thermal decomposition of dicarboxylic acids, and is a marker of highly oxygenated and processed organic material (Zhang et al., 2007; Ng et al., 2010; Morgan et al., 2010). This mass fragment comprises 27% of the total organic mass fraction in the coastal zone and 25% in the remote zone suggesting that a significant proportion of the aerosol are predominantly oxidized.

An indication of the neutrality of aerosol can be drawn from the molar mass ratio between ammonium and sulphate measured by the AMS. This is plotted for the FT and MBL from all aircraft in Fig. 8 as a function of longitude along 20° S and colour-scaled

for sulphate mass concentration. A value less than unity indicates that there are insufficient ammonium ions to fully balance sulphate ions indicating potentially acidic aerosol unless aerosol are otherwise buffered. A value between one and two may indicate partially neutralised aerosol, whilst a value greater than two likely indicates full neutrality. The limits of these thresholds are plotted as a dashed green line in Fig. 8. To avoid potential systematic biases associated with AMS retrievals near to the limit of detection, only data where mass loadings exceed 0.2 µg m^{-3} in the case of sulphate and 0.0375 µg m^{-3} in the case of ammonium, are considered. In Fig. 8 we see that the majority of aerosol at all longitudes is often highly acidic or only partially buffered by ammonium. A linear fit (though with poor confidence) to the data indicates a very weak increasing gradient in molar ratio with longitude, and the change from red to blue colouring with longitude illustrates the reduction in sulphate loading with distance offshore observed in Fig. 7. A similar pattern is seen in the FT. However, R^2 correlation coefficients for fits to data in the MBL and FT in Fig. 8 are noted to be poor at 0.2 and 0.17, respectively. Sources of ammonium aerosol near to shore are not well known. It may be possible that there is a hitherto unidentified ammonium source very near to the shoreline. Elevated ammonium loading appears limited to the near-shore and therefore may not pose a significant factor in the context of cloud chemistry along the wider 20° S parallel.

Another source for balance between ammonium and sulphate could be the presence of MSA, which was detected by the VACC system on the BAe-146 and has a significant marine source as discussed earlier. The VACC system is capable of resolving sea-salt and other material to which the AMS is not sensitive. In total, 33 VACC scans were selected from flights B408, B410, B412, B414, B415, and B417 and zonal averages were calculated after dividing measurements into coastal, transition and remote zones as discussed earlier. In this study, the following species were identified by volatility analysis and are summarised in Table 3: organic species with volatilization temperatures below 105 °C (denoted as Org), organic compounds with volatilization temperatures between 140 and 150 °C (denoted as VOC), ammonium bisulphate (AHS), methane

sulphonic acid (MSA), ammonium nitrate (AN), ammonium sulphate (AS), and core particles (such as sea-salt and mineral dust) with volatilization temperatures are above 750 °C.

A particle number concentration gradient was observed for ambient VACC measurements (i.e., volatilization temperatures below 80 °C) in the size range 110–500 nm over the 20° S parallel with concentrations of 138, 97, and 70 cm^{-3} for the coast, transition and remote zones, respectively. Table 3 displays the zonal mean particle number concentration integrated over the diameter range 110–500 nm and expressed as percentage of the VACC total particle number concentration for the identified chemical species. For all zones, the dominant compound in terms of number concentration is AS, which is consistent with conclusions drawn from AMS measurements. Core (6.3–8.3 %) and MSA (17.4–20.1 %) particles contribute in similar fashion to the particle number concentration. The percentage of particle number concentration containing AS gradually decreases from the coast (58.5%) towards the remote region (41.4%), consistent with the decreasing ammonium-to-sulphate molar ratio observed by the AMS. Proportionally, the contribution from AN slightly increases towards the remote region (5.9–10.2 %), although the overall concentration of particles decreases with distance from shore. The core component gives an indication of the sea-salt and mineral dust fraction, suggesting that less than 10% of measured particles were thus composed.

Figure 9 shows a campaign-average humidogram calculated from data recorded in the MBL across all longitude zones (no systematic change with longitude was identified) by a wet Nephelometer on the BAe-146 as the ratio of the scattering of the aerosol at a given RH to the scattering of the dry aerosol. Only those aerosol of size less than the transmission cut-off of the Rosemount inlet (<2 µm) were sampled, thus representing the bulk of CCN active particles. Black points represent the mean of all data sampled at 1Hz and gridded into bins of 2% relative humidity (RH) along with upper and lower quartile whiskers. A theoretical curve for ammonium sulphate is plotted as a solid black line for reference and a dashed line illustrates a growth curve more typical of what is observed in European pollution over the UK, which tends to be a mixture

of ammonium sulphate, ammonium nitrate and organics (see Haywood et al., 2008). From this, we see that the increase in scattering with RH (f(RH)) of MBL sub-micron aerosol is consistent with an ammonium sulphate composition in agreement with AMS and VACC measurements.

In summary, we believe that correlated sources of CO and aerosol composition in the coastal zone represent an aged continental combustion origin with contributions from local and regional agriculture and biology. The transition region exhibits reduced concentrations and variability. The remote zone is relatively clean in terms of non-refractory aerosol throughout and exhibits a background state – we conclude that the remote region sulfate and ammonium aerosol mass is comprised of marine biogenic sources, with organic mass perhaps elevated due to entrainment. Aerosol composition is broadly consistent with a mix of acidic sulphate aerosol with some ammonium sulphate and MSA.

4.4 Bulk aerosol and cloud properties

The relationship between aerosol size and composition, atmospheric thermodynamics and cloud properties are non-linear and beyond the scope of this paper. Future modeling studies will aim to address such sensitivities, with the analysis here aiming to inform such activity. However, for relation to composition statistics presented in Fig. 4, we present aerosol number statistics and cloud droplet number as a function of longitude in Fig. 10 for the MBL and FT in the left and right panels, respectively, with the exception that cloud droplet number is not reported for the FT (since this is above cloud top). In the figure, ACN refers to aerosol number concentration between 40 nm and 3 µm particle diameter; CCN refers to activated condensation nuclei colour-coded for supersaturation; CDN refers to cloud droplet number measured by the CDP on the BAe-146 and NSF-C130; and CAPS on the DoE-G1; and CN refers to total condensation nuclei measured by CPC instruments. Sampling statistics are given above each longitude bin in each panel. In the MBL, correlated gradients in CCN, CND, CN and ACN are all observed, with a near-equivalent quantitative relationship between ACN and CDN

near the coast, suggesting that the majority of sub-micron aerosol (with number modes noted to be around 150 nm, see next section) may be activated in cloud. Furthermore, analysis of CCN number suggests that aerosol are activated at low super-saturations (0.11%), though this conclusion does not take account of potential influences due to updraught speed.

Comparing the FT (right panel of Fig. 10) with the MBL (left panel of Fig. 10), we see that CN are enhanced near the coast, with no significant increase in ACN. This suggests that the CN near the coast are dominated by very small particles (<40 nm). This increase in CN near the coast displays a similar character to the SO_2 statistics seen in Fig. 4, suggesting that outflow of SO_2 into the FT leads to new nucleation in the coastal FT.

We also note an evident increase in ACN variability in the FT to the west of 80° W, which is co-located with an increase in CO and organic aerosol mass concentration discussed earlier and seen in Figs. 4 and 7. This is consistent with biomass burning plumes which carry elevated CO and organic combustion aerosol. A slight increase in ACN in the MBL is also noted at this location.

4.5 Aerosol number size distributions

Mean aerosol number concentration spectra, normalized for bin width recorded by aerosol spectrometers on all aircraft platforms in the MBL and FT are plotted in Fig. 11 and represent averaged spectra normalized for bin width in the coastal, transition and remote zones as labeled in the figure. One standard deviation are also plotted for each longitude zone and the total sampling time is given in each panel.

In order for this aerosol size climatology to be easily used by the reader we have also fitted up to four log-normal modes to each spectrum (continuous smooth black lines in each panel) according to the following relationship described further by Pruppacher and Klett (1997):

$$\frac{dN}{dD} = \frac{N_{\text{tot}}}{D\sqrt{2\pi}\ln\sigma_{\text{g}}}\exp\left(\frac{\ln^2\frac{D}{D_{\text{g}}}}{2\ln^2\sigma_{\text{g}}}\right) \quad (1)$$

where N_{tot} is the particle number concentration (in particles cm^{-3}), D is the particle diameter (μm), and D_{g} and σ_{g} are the number median diameter and the geometric standard deviation of the modal distribution, respectively. For each aerosol size spectrum, three modes were fitted to the sub-micron component and one to the coarse (super-micron) component in the range 10 nm and 5 μm. An interactive routine was written to fit the log-normal modes to the size distribution data. These approximate fits were used as an initial guess in a Gauss-Newton non-linear fitting technique to yield the best fit to the data by minimising the chi-square error on successive iterations. The convergent log-normal parameters and confidences for each spectrum in Fig. 11 are given in Table 4.

Figure 11 shows aerosol particle number concentrations normalised to the natural logarithm of bin width (note that this is in-line with the equation above for consistency though some readers may be more familiar with such spectra normalised to a base 10 logarithm) a variation in modality between the coast and remote zones in the MBL with a consistently dominant accumulation mode between 150 nm to 190 nm in all zones, peaking at 170 nm, except for the remote MBL zone, which has a stronger accumulation mode (in terms of number, not mass) at 35 nm. The 150 nm mode in the all MBL zones peaks at between 325 and 375 cm^{-3}, with the lowest peak concentration in the remote zone. The reduction in the 150 nm number mode with distance offshore appears to favour the growth of new aerosol in the region, with the appearance of an Aitken mode at 35 nm in both the transition and remote MBL zones. A further weak mode at 15 nm in the coastal MBL zone may indicate more recent nucleation. Turning our attention to the FT (right panels of Fig. 11), we see a much sharper difference with longitude (though data are not available for the remote zone FT). In the coastal FT, we see an accumulation mode shifted to 100 nm and a much more prevalent mode (in terms of

number) at 15 nm. The presence of the same 15 nm mode in the coastal MBL, seen in the standard deviation curve superimposed on the mean spectra, may again signify entrainment of this mode through cloud top. Similarly, in the transition FT region, we see a mode at 25 nm, simultaneous with the elevation of this mode in the MBL beneath.

The standard deviation of the peak number concentration is seen to vary typically by a factor of two around the mean (grey bars in Fig. 11). Furthermore, the coarse mode, measured by PCASP instruments on all aircraft appears to be highly variable in the coast and transition MBL zones, seen as the wide grey bars on Fig. 11 for example. This is due to the high natural variability in the coarse mode, perhaps due to sea-salt sampled on near surface aircraft runs. Coarse mode variability is seen to be much reduced in the remote MBL zone and absent in the FT, consistent with the expectation that the FT is essentially void of such aerosol in the background state (volcanic emissions notwithstanding).

Figures 12 and 13, shows similarly averaged aerosol spectra from the Paposo and Paranal surface sites, respectively. In Fig. 12, the data have been divided into early morning (03:00–05:00 a.m. local time) and mid-afternoon (03:00–05:00 p.m.) periods between 15 October and 31 October (defined here as period 1) and 1 November to 15 November (defined as period 2), 2008, to examine diurnal differences in up-and-down-slope advection and differences between the synoptic meteorological regimes discussed in Sect. 4.1. There is little difference in the aerosol spectra at Paposo in the morning or afternoon in late October, with peaks in accumulation mode aerosol observed at 50 nm and 150 nm, consistent with aircraft measurements in the coastal FT at this time. The afternoon spectra in period 2 are much like those in period 1, however there is a significant difference between the morning and afternoon spectra in early November, with the clear observation of a highly variable mode at 20 nm in the morning which is absent in the afternoon. The early morning period is characterised by down-slope advection and sampling of air which has subsided over the Andes PBL overnight. We are reminded of the 20 nm mode observed in Fig. 11 in the coastal FT. This would suggest that air sampled in down-slope advection at Paposo is indeed

similar in terms of aerosol chemistry to that sampled in the coastal FT. Interestingly, this 20 nm mode is entirely absent from similar data recorded at lower altitude at Paranal (see Fig. 13), which sees a relatively invariant peak mode at 100 nm. Paranal is located 15 km inland at 2635 m a.s.l. on the steep slopes of the Andes. A potential reason for the observation of the 20 nm mode at Paranal, yet not at Paposo, could be related to the reduction in accumulation mode aerosol at the top of the PBL by cloud formation and subsequent nucleation of new Aitken mode aerosol which is then advected down slope. The reason for the observation of a 25 nm mode at Paposo in early November and not in late October is not clear but may be related to the contrasting strength of the synoptic subtropical anticyclone as diagnosed in Sect. 4.1, which may act to modulate cloud formation over the slopes of the Andes in the region of Paranal.

In summary, a dominant (in terms of number) but variable accumulation mode is observed between 150 nm and 190 nm in all locations in the MBL, with the exception of the remote zone, which has peaks at 35 and 150 nm. The strength of this mode reduces with distance offshore in both periods, consistent with gradients in other tracers and airmass origins discussed earlier. Evidence of recent nucleation is observed near to shore in the FT and correlated modes in the MBL in all zones suggest that entrainment is a significant process. Observation of surface site aerosol spectra give some insight into diurnal coastal dynamics and processes, with the observation of a characteristic 25 nm mode in down-slope advection at Paposo in the early morning, which is noted to be absent in the up-slope advection in the mid-afternoon.

5 Conclusions

This paper presents a climatology of selected chemical tracers and aerosol size and composition statistics in the marine boundary layer and an above-cloud layer between 1700 m and 3200 m altitude above the South East Pacific as measured onboard aircraft, the Ronald H Brown cruise ship and surface aerosol sites along the 20° S parallel as part of the VOCALS-REx field campaign between 15 October 2008 and

15 November 2008. The climatology is interpreted in the context of airmass origins and emission sources relevant to cloud chemistry and microphysics and modelling activity.

Significant zonal gradients in MBL carbon monoxide and ozone, aerosol number, aerosol size and aerosol composition were observed in the mean over the course of the campaign, with a generally more variable and polluted coastal MBL environment and a less variable, cleaner remote maritime MBL background. Generalised back trajectory analysis demonstrates that the observed zonal gradients in the boundary layer are characteristic of marked changes in airmass history with distance offshore – coastal boundary layer airmasses having been in recent contact with the regional land surface, whilst remote maritime airmasses reside over ocean for in excess of 10 days. Boundary layer composition is seen to be dominated by sulphate and surface coastal emissions of sulphur near to shore, but also by episodic entrainment of polluted free tropospheric layers through cloud top.

Free tropospheric airmass history is seen to be more variable than that in the boundary layer, with a complex interleaving of layers from diverse source regions overlaid in the vertical. The FT is generally more polluted in the mean than the MBL in terms of ozone, SO_2 and ozone and is characterised dynamically by both rapid descent of airmasses transported rapidly and long-range in the southern subtropical jetstream from Australasia. Elevated ozone in the FT is perhaps due to mixing with the ozone-rich tropical tropopause layer. The composition of the coastal FT is further complicated by near-coastal dynamics such as Andean pumping, with elevated SO_2 noted in the FT near to shore, suggesting the potential influence of large mining smelters on coastal FT airmasses.

A dominant aerosol accumulation mode between 150 nm and 190 nm was observed throughout in the MBL, with the exception of the remote zone, which exhibited a strong additional Aitken mode at 35 nm. In the FT, an accumulation mode at 100 nm was observed in the coastal zone, as well as a stronger Aitken mode (in terms of number) at 15 nm, which may suggest recent nucleation following the removal of the accumulation mode perhaps by cloud processing.

As previously documented, cloud droplet number is well correlated with accumulation mode aerosol number and is consistent with complete activation of the 150 nm accumulation mode aerosol at low super-saturations.

The climatology presented here aims to provide a valuable dataset to inform model simulation, particularly in the context of aerosol-cloud interaction and evaluation of dynamical processes in the SEP region for conditions analogous to those during VOCALS-REx.

Appendix A

List of acronyms

ACN	Accumulation mode aerosol (sub-micron diameter particles)
AHS	Ammonium bisulphate
AMS	Aerosol mass spectrometer
AMSL	above mean sea level
AN	Ammonium nitrate
AS	Ammonium sulphate
CAPS	Cloud aerosol spectrometer probe
CCN	Cloud condensation nuclei
CDN	Cloud droplet number
CDP	Cloud droplet probe
CN	Condensation nuclei
CPC	Condensation particle counter
CVI	Counterflow virtual impactor
DMA	Differential mobility analyser
DMPS	Differential mobility particle sampler

DMS	Dimethyl sulphide
FT	Free troposphere
GPS	Global positioning system
LWC	Liquid water content
MBL	Marine boundary layer
MSA	Methyl sulphonic acid
OPC	Optical particle counter
PBL	Planetary boundary layer
PDF	Probability density function
PCASP	Passive cavity aerosol spectrometer probe
SEP	South East Pacific
SMPS	Scanning mobility particle sampler
SST	Sea surface temperature
VACC	Volatility Analyser
VAMOS	Variability in the American monsoon system
VOC	Volatile organic compound
VOCALS-REx	VAMOS Ocean-cloud-atmosphere land study – regional experiment

Acknowledgements. We are extremely grateful to the support staff, crew and scientists who helped make the VOCALS-REx a success. These include the PIs, support scientists and crews of the six aircraft platforms (the NSF/NCAR C-130, the UK FAAM BAe-146, the DoE G-1, the CIRPAS Twin Otter, the UK NERC Dornier 228, and, in the 2010 CUpEx phase, the Chilean DGAC King Air), the research vessel NOAA Ronald H. Brown, and the land stations at Iquique and Paposo. The NCAR Earth Observing Laboratory is thanked for their dedication to coordinating and executing field logistics and data archive support for VOCALS Rex. We thank NERC for funding the VOCALS UK contingent to the project (ref: NE/F019874/1) and the NERC Facility for Airborne and Atmospheric Measurment (FAAM) and Direct Flight and Avalon for operational support of the BAe-146 aircraft. We also thank the British Atmospheric Data Centre for archiving of ECMWF operational analysis data. We also thank the FORMAS agency for funding and the European Southern Observatory (ESO) for support of the surface site activities.

References

Aiken, A. C., DeCarlo, P. F., Kroll, J. H., Worsnop, D. R., Huffman, J. A., Docherty, K., Ulbrich, I. M., Mohr, C., Kimmel, J. R., Sueper, D., Zhang, Q., Sun, Y., Trimborn, A., Northway, M., Ziemann, P. J., Canagaratna, M. R., Onasch, T. B., Alfarra, R., Prevot, A. S. H., Dommen, J., Duplissy, J., Metzger, A., Baltensperger, U., and Jimenez, J. L.: O/C and OM/OC ratios of primary, secondary, and ambient organic aerosols with high-resolution time-of-flight aerosol mass spectrometry, Env. Sci. Technol., 42, 4478–4485, 2008. 692

Allan, J. D., Jimenez, J. L., Williams, P. I., Alfarra, M. E., Bower, K. N., Jayne, J. T., Coe, H., and Worsnop, D. R.: Quantitative sampling using an aerodyne mass spectrometer 1, techniques of data interpretation and error analysis, J. Geophys. Res., 108(D3), 4090–4099, 2003. 690, 692

Allan, J. D., Coe, H., Bower, K. N., Alfarra, M. E., Delia, A. E., Jimenez, J. L., Middlebrook, A. M., Drewnick, F., Onasch, T. B., Canagaratna, M. R., Jayne, J. T., and Worsnop, D. R.: A generalised method for the extraction of chemically resolved mass spectra from Aerodyne aerosol mass spectrometer data, J. Aerosol Sci., 35, 909–922, 2004a. 690, 692

Allan, J. D., Bower, K. N., Coe, H., Boudries, H., Jayne, J. T., Canagaratna, M. R., Millet, D. B., Goldstein, A. H., Quinn, P. K., Weber, R. J., and Worsnop, D. R.: Submicron aerosol composition at Trinidad Head, California, during ITCT 2K2: its relationship with gas phase volatile organic carbon and assessment of instrument performance, J. Geophys. Res., 109, 2004b.

Allan, J. D., Baumgardner, D., Raga, G. B., Mayol-Bracero, O. L., Morales-García, F., García-García, F., Montero-Martínez, G., Borrmann, S., Schneider, J., Mertes, S., Walter, S., Gysel, M., Dusek, U., Frank, G. P., and Krämer, M.: Clouds and aerosols in Puerto Rico – a new evaluation, Atmos. Chem. Phys., 8, 1293–1309, doi:10.5194/acp-8-1293-2008, 2008. 709

Allan, J. D., Topping, D. O., Good, N., Irwin, M., Flynn, M., Williams, P. I., Coe, H., Baker, A. R., Martino, M., Niedermeier, N., Wiedensohler, A., Lehmann, S., Müller, K., Herrmann, H., and McFiggans, G.: Composition and properties of atmospheric particles in the eastern Atlantic and impacts on gas phase uptake rates, Atmos. Chem. Phys., 9, 9299-9314, doi:10.5194/acp-9-9299-2009, 2009. 708

Allen, G., Vaughan, G., Bower, K. N., Williams, P. I., Crosier, J., Flynn, M., Connolly, P., Hamilton, J. F., Lee, J. D., Saxton, J. E., Watson, N. M., Gallagher, M., Coe, H., Allan, J., Choularton, T. W., and Lewis, A. C.: Aerosol and trace-gas measurements in the Darwin area during the wet season, J. Geophys. Res., 113, D06306, doi:10.1029/2007JD008706, 2007. 703,

704, 708
Ayers, G. P., Ivey, J. P., and Gillett, R. W.: Coherence between seasonal cycles of dimethyl sulfide, methanesulfonate and sulfate in marine air, Nature, 349, 404–406, 1991. 709
Baron, P. A. and Willeke, K. (Eds.): Aerosol Measurement: Principles, Techniques, and Applications, Van Nostrand Reinhold, New York, 179–180, 1993. 688
Bates, T. S., Quinn, P. K., Coffman, D., Schulz, K., Covert, D. S., Johnson, J. E., Williams, E. J., Lerner, B. M., Angevine, W. M., Tucker, S. C., Brewer, W. A., and Stohl, A.: Boundary layer aerosol chemistry during TexAQS/GoMACCS 2006: insights into aerosol sources and transformation processes, J. Geophys. Res., 113, D00F01, doi:10.1029/2008JD010023, 2008. 694, 729
Bony, S. and Dufresne, J. L.: Marine boundary layer clouds at the heart of tropical cloud feedback uncertainties in climate models, Geophys. Res. Lett., 32, L20806, doi:10.1029/2005GL023851, 2005. 684
Bretherton, C. S., Peters, M. E., and Back, L. E.: Relationships between water vapor path and precipitation over the Tropical Oceans, J. Climate, 17, 1517–1528, 2004. 686
Bretherton, C. S., Wood, R., George, R. C., Leon, D., Allen, G., and Zheng, X.: Southeast Pacific stratocumulus clouds, precipitation and boundary layer structure sampled along 20° S during VOCALS-REx, Atmos. Chem. Phys., 10, 10639–10654, doi:10.5194/acp-10-10639-2010, 2010. 687, 698, 701
Brooks, B. J., Smith, M. H., Hilla, M. K., and O'Dowdb, C. D.: Size-differentiated volatility analysis of internally mixed laboratory-generated aerosol, J. Aerosol Sci. , 33, 555–579, 2002. 690, 729
Brooks, B. J., McQuaid, J. B., Smith, M. H., Crosier, J., Williams, P. I., Coe, H., and Osborne, S. R.: Inter-comparison of VACC and AMS derived nitrate, sulphate and ammonium aerosol loadings during ADRIEX, Q. J. Roy. Meteorol. Soc., 133(S1), 77–84, 2007. 690
Carn, S. A., Krueger, A. J., Krotkov, N. A., Yang, K., and Levelt, P. F.: Sulfur dioxide emissions from Peruvian copper smelters detected by the ozone monitoring instrument, Geophys. Res. Lett., 34, L09801, doi:10.1029/2006GL029020, 2007. 703
Clarke, A. and Kapustin, V.: Hemispheric aerosol vertical profiles: anthropogenic impacts on optical depth and cloud nuclei, Science, 329(5998), 1488–1492, 2010. 692, 701, 702, 707
Crosier, J., Allan, J. D., Coe, H., Bower, K. N., Formenti, P., and Williams, P. I.: Chemical composition of summertime aerosol in the Po Valley (Italy), Northern Adriatic and Black Sea, Q. J. Roy. Meteorol. Soc., 133, 61–75, 2007. 691

Collins, D. R., Flagan, R. C., and Seinfeld, J. H.: Improved inversion of scanning DMA data, Aerosol Sci. Tech., 36(1), 1–9, 2002. 693
DeCarlo, P. F., Kimmel, J. R., Trimborn, A., Northway, M. J., Jayne, J. T., Aiken, A. C., Gonin, M., Fuhrer, K., Horvath, T., Docherty, K., Worsnop, D. R., and Jiménez, J. L.: Field-deployable, high-resolution, time-of-flight aerosol mass spectrometer, Anal. Chem., 78(24), 8281–8289, 2006. 692, 729
de Szoeke, S. P., Fairall, C. W., and Pezoa, S.: Ship Observations of the Tropical Pacific Ocean along the Coast of South America, J. Climate, 22, 45864, doi:10.1175/2008JCLI2555.1, 2009. 686
Drewnick, F., Hings, S., and Decarlo, P.: A new Time-of-Flight Aerosol Mass Spectrometer (TOF-AMS)-instrument description and first field deployment, Aerosol Sci. Tech., 39, 637–658, 2005. 690
Facchini, M. C., Decesari, S., Rinaldit, M., Carbone, C., Finessi, E., Mircea, M., Fuzzi, S., Moretti, F., Tagliavini, E., Ceburnis, D., and O'Dowd, C. D.: Important source of marine secondary organic aerosol from biogenic amines, Environ. Sci. Technol., 42, 9116–9121, doi:10.1021/es8018385, 2008. 709
Feingold, G., Cotton, W. R., Kreidenweis, S. M., and Davis, J. T.: Impact of giant cloud condensation nuclei on drizzle formation in stratocumulus: implications for cloud radiative properties, J. Atmos. Sci., 56, 4000–4117, 1999. 707
Garreaud, D. and Munoz, R. C.: The low-level jet off the west coast of subtropical South America: structure and variability, Mon. Weather Rev., 133, 2246–2261, 2005. 685
Gerbig, C., Schmitgen, S., Kley, D., Volz-Thomas, A., Dewey, K., and Haaks, D.: An improved fast-resposse VUV resonance flourescence CO instrument, J. Geophys. Res., 104, 1699–1704, 1999. 689
Hannay, C., Williamson, D. L., Hack, J. J., Kiehl, J. T., Olson, J. G., Klein, S. A., Bretherton, C. S., and Köhler, M.: Evaluation of forecasted southeast pacific stratocumulus in the NCAR, GFDL, and ECMWF models, J. Climate, 22, 2871–2889, doi:10.1175/2008JCLI2479.1, 2009. 685
Haywood, J., Bush, M., and Abel, S.: Prediction of visibility and aerosol within the operational Met Office Unified Model. II: validation of model performance using observational data, Q. J. Roy. Meteorol. Soc., 134, 1817–1832, doi:10.1002/qj.275, 2008. 712
Heyes, W. J., Vaughan, G., Allen, G., Volz-Thomas, A., Ptz, H.-W., and Busen, R.: Composition of the TTL over Darwin: local mixing or long-range transport?, Atmos. Chem. Phys., 9, 7725–

7736, doi:10.5194/acp-9-7725-2009, 2009. 708
Huebert, B. J., Howell, S. G., Covert, D., Bertram, T., Clarke, A., Anderson, J. R., Lafleur, B. G., Seebaugh, W. R., Wilson, J. C., Gesler, D., Blomquist, B., and Fox, J.: PELTI: Measuring the passing efficiency of an airborne low turbulence aerosol inlet, Aerosol Sci. Tech., 38(8), 803–826, 2004. 691
Huneeus, N., Gallardo, L., and Rutllan, J. A.: Offshore transport episodes of anthropogenic sulfur in Northern Chile: potential impact on the stratocumulus cloud deck, Geophys. Res. Lett., 33, L19819, doi:10.1029/2006GL026921, 2006. 685, 707
Jayne, J. T., Leard, D. C., Zhang, X. F., Davidovits, P., Smith, K. A., Kolb, C. E., and Worsnop, D. R.: Development of an aerosol mass spectrometer for size and composition analysis of submicron particles, Aerosol Sci. Tech., 33, 1, 49–70, 2000. 690, 729
Jimenez, J. L., Jayne, J. T., Shi, Q., Kolb, C. E., Worsnop, D. R., Yourshaw, I., Seinfeld, J. H., Flagan, R. C., Zhang, X., Smith, K. A., Morris, J. W., and Davidovits, P.: Ambient aerosol sampling using the aerodyne mass spectrometer, J. Geophys. Res., 108(D7), 8425–8437, doi:10.1029/2001JD001213, 2003. 690
Kollias, P., Fairall, C. W., Zuidema, P., Tomlinson, J., and Wick, G. A.: Observations of marine stratocumulus in SE Pacific during the PACS 2003 cruise, Geophys. Res. Lett., 31, L22110, doi:10.1029/2004GL020751, 2004. 686
Kleinman, L. I., Daum, P. H., Lee, Y.-N., Senum, G. I., Springston, S. R., Wang, J., Berkowitz, C., Hubbe, J., Zaveri, R. A., Brechtel, F. J., Jayne, J., Onasch, T. B., and Worsnop, D.: Aircraft observations of aerosol composition and ageing in New England and Mid-Atlantic States during the summer 2002 New England air quality study field campaign, J. Geophys. Res., 112, D09310, doi:10.1029/2006JD007786, 2007. 693
Kleinman, L. I.: Aerosol concentration and size distribution measured below, in, and above cloud from the DOE G-1 during VOCALS, in preparation, 2010. 693
Lefohn, A. S., Oltmans, S. J., Dann, T., and Singh, H. B.: Present-day variability of background ozone in the lower troposphere. J. Geophys. Res., 106(D9), 9945–9958, doi:10.1029/2000JD900793, 2001. 704
Loyola, D., Van Geffen, J., Valks, P., Erbertseder, T., Van Roozendael, M., Thomas, W., Zimmerm, W., and Wißkirchen, K.: Satellite-based detection of volcanic sulphur dioxide from recent eruptions in Central and South America, Adv. Geosci., 14, 35–40, 2008, http://www.adv-geosci.net/14/35/2008/. 703
Ma, C.-C., Mechoso, C. R., Robertson, A. W., and Arakawa, A.: Peruvian stratus clouds and the

Tropical Pacific circulation: a coupled ocean-atmosphere GCM study, J. Climate, 9, 1635–1645, 1996. 685
Mari, C., Suhre, K., Bates, T. S., Johnson, J. E., Rosset, R., Bandy, A. R., Eisele, F. L., Mauldin, R. L., and Thornton, D. C.: Physico-chemical modeling of the first aerosol Characterization Experiment (ACE 1) lagrangian B. 2. DMS emission, transport and oxidation at the mesoscale: first Aerosol Characterization Experiment (ACE 1), J. Geophys. Res., 103(D13), 16457–16473, 1998. 709
Matthew, B. M., Middlebrook, A. M., and Onasch, T. B.: Collection efficiencies in an aerodyne aerosol mass spectrometer as a function of particle phase for laboratory generated aerosols, Aerosol Sci. Tech., 42(11), 884–898, 2008. 691
McFarlane, D. A., Keeler, R. C., and Mizutani, H.: Ammonia volatilization in a Mexican bat cave ecosystem, Biogeochemistry, 30(1), 1–8, doi:10.1007/BF02181037, 1995.
McNaughton, C. S., Clarke, A. D., Howell, S. G., Pinkerton, M., Anderson, B., Thornhill, L., Hudgins, C., Winstead, E., Dibb, J. E., Scheuer, E., and Maring, H.: Results from the DC-8 Inlet Characterization Experiment (DICE): airborne versus surface sampling of mineral dust and sea salt aerosols, Aerosol Sci. Tech., 41(2), 136–159, 2007. 691
Mechoso, C. R., Robertson, A. W., Barth, N., Davey, M. K., Delecluse, P., Gent, P. R., Ineson, S., Kirtman, B., Latif, M., Le Treut, H., Nagai, T., Neelin, J. D., Polcher, J., Stockdale, T., Terray, L., Thual, O., and Tribbia, J. J.: The seasonal cycle over the Tropical Pacific in general circulation models, Mon. Weather Rev., 123, 2825–2838, 1995. 686
Meehl, G. A., Stocker, T. F., Collins, W. D., Friedlingstein, P., Gaye, A. T., Gregory, J. M., Kitoh, A., Knutti, R., Murphy, J. M., Noda, A., Raper, S. C. B., Watterson, I. G., Weaver, A. J., and Zhao, Z.-C.: Global climate projections, in: Climate Change 2007: The Physical Science Basis. Contribution of Working Group I to the Fourth Assessment Report of the Intergovernmental Panel on Climate Change, edited by: Solomon, S., Qin, D., Manning, M., Chen, Z., Marquis, M., Averyt, K. B., Tignor, M., and Miller, H. L., Cambridge University Press, Cambridge, UK and New York, NY, USA, 2007. 684
Morgan, W. T., Allan, J. D., Bower, K. N., Esselborn, M., Harris, B., Henzing, J. S., Highwood, E. J., Kiendler-Scharr, A., McMeeking, G. R., Mensah, A. A., Northway, M. J., Osborne, S., Williams, P. I., Krejci, R., and Coe, H.: Enhancement of the aerosol direct radiative effect by semi-volatile aerosol components: airborne measurements in North-Western Europe, Atmos. Chem. Phys., 10, 8151–8171, doi:10.5194/acp-10-8151-2010, 2010. 709
Ng, N. L., Canagaratna, M. R., Zhang, Q., Jimenez, J. L., Tian, J., Ulbrich, I. M., Kroll, J. H.,

Docherty, K. S., Chhabra, P. S., Bahreini, R., Murphy, S. M., Seinfeld, J. H., Hildebrandt, L., Donahue, N. M., DeCarlo, P. F., Lanz, V. A., Prvt, A. S. H., Dinar, E., Rudich, Y., and Worsnop, D. R.: Organic aerosol components observed in Northern Hemispheric datasets from Aerosol Mass Spectrometry, Atmos. Chem. Phys., 10, 4625-4641, doi:10.5194/acp-10-4625-2010, 2010. 709

Norman, A. L. and Wadleigh, M. A.: Dimethyl Sulphide (DMS) and its Oxidation to Sulphur Dioxide Downwind of an Ocean Iron Fertilization Study, SERIES: A Model for DMS Flux, Air Pollution Modeling and Its Application XVII, 3, 237–244, DOI: 10.1007/978-0-387-68854-126, 2007. 703

Novakov, T., Corrigan, C. E., Penner, J. E., Chuang, C. C., Rosario, O., and Mayol-Bracero, O. L.: Organic aerosols in the Caribbean trade winds: a natural source?, J. Geophys. Res.-Atmos., 102, 21307–21313, 1997. 709

Novakov, T. and Penner, J. E.: Large contribution of organic aerosols to cloud-condensation nuclei concentrations, Nature, 365, 823–826, 1993. 709

O'Dowd, C. D., Facchini, M. C., Cavalli, F., Ceburnis, D., Mircea, M., Decesari, S., Fuzzi, S., Yoon, Y. J., and Putaud, J. P.: Biogenically driven organic contribution to marine aerosol, Nature, 431, 676–680, 2004. 709

Pruppacher, H. P. and J. D. Klett (Eds.): Microphysics of Clouds and Precipitation, Kluwer Academic Press, Dordrecht, The Netherlands, 26 pp., 1997. 713

Raes, F., Van Dingenen, R., Vignati, E., Wilson, J., Putaud, J. P., Seinfeld, J. H., and Adams, P.: Formation and cycling of aerosols in the global troposphere, Atmos. Environ., 34, 4215–4240, 2000. 709

Rahn, D. A. and Garreaud, R.: Marine boundary layer over the subtropical southeast Pacific during VOCALS-REx – Part 1: Mean structure and diurnal cycle, Atmos. Chem. Phys., 10, 4491–4506, doi:10.5194/acp-10-4491-2010, 2010. 699

Rahn, D. A. and Garreaud, R.: Marine boundary layer over the subtropical southeast Pacific during VOCALS-REx – Part 2: Synoptic variability, Atmos. Chem. Phys., 10, 4507–4519, doi:10.5194/acp-10-4507-2010, 2010. 699

Randall, D. A., Wood, R. A., Bony, S., Colman, R., Fichefet, T., Fyfe, J., Kattsov, V., Pitman, A., Shukla, J., Srinivasan, J., Stouffer, R. J., Sumi, A., and Taylor, K. E.: Cilmate models and their evaluation, in: Climate Change 2007: the Physical Science Basis, Contribution of Working Group I to the Fourth Assessment Report of the Intergovernmental Panel on Climate Change, edited by: Solomon, S., Qin, D., Manning, M., Chen, Z., Marquis, M., Averyt, K. B.,

Tignor, M., and Miller, H. L., Cambridge University Press, Cambridge, UK and New York, NY, USA. 2007. 684

Richter, I. and Mechoso, C. R.: Orographic influences on subtropical stratocumulus, J. Atmos. Sci., 63(10), 2585–2601. 2006. 685

Romo-Krögera, C. M., Moralesa, J. R., Dinatora, M. I., Llonaa, F., and Eaton, L. C.: Heavy metals in the atmosphere coming from a copper smelter in Chile, Atmos. Env., 28(4), 705–711, doi:10.1016/1352-2310(94)90047-7, 1994. 706

Serpetzoglou, E., Albrecht, B. A., Kollias, P., and Fairall, C. W.: Boundary layer, cloud, and drizzle variability in the Southeast Pacific stratocumulus regime, J. Climate, 21, 6191–6214, doi:10.1175/2008JCLI2186.1, 2008 686

Springston, S. R., Kleinman, L. I., Nunnermacker, L. J., Brechtel, F., Lee, Y.-N., and Wang, J.: Chemical evolution of an isolated power plant plume during the TexAQs 2000 study, Atmos. Environ. 39, 3431–3443, 2005. 693

Staudt, A. C., Jacob, D. J., Bachiochi, D., Krishnamurtiand, T. N., Sachse, G. W., and Logan, J.: Continental sources, transoceanic transport, and inter-hemispheric exchange of carbon monoxide over the Pacific, J. Geophys. Res., 106(D23), 32571–32590, 2001 703

Tang, I. N. and Munkelwitz, H. R.: Chemical and size effects of hygroscopic aerosols on light scattering coefficients, J. Geophys. Res., 101, 19245–19250, 1996. 689

Tomlinson, J. M., Li, R., and Collins, D. R.: Physical and chemical properties of the aerosol within the Southeastern Pacific marine boundary layer, J. Geophys. Res., 112, D12211, doi:10.1029/2006JD007771., 2007. 685

Toniazzo, T.: Climate variability in the South-Eastern Tropical Pacific and its relation with ENSO: a GCM study, Climate Dynam., 34(7–8), 1093–1114, doi:10.1007/s00382–009-0602, 2010. 699

Topping, D. O., McFiggans, G. B., and Coe, H.: A curved multi-component aerosol hygroscopicity model framework: Part 2 – Including organic compounds, Atmos. Chem. Phys., 5, 1223–1242, doi:10.5194/acp-5-1223-2005, 2005. 696

Wang, S. C. and Flagan, R. C.: Scanning electrical mobility spectrometer, Aerosol Sci. Tech., 13, 230–240, 1990 689, 729

Wood, R., Bretherton, C. S., Mechoso, C. R., Weller, R. A., Huebert, B., Straneo, F., Albrecht, B. A., Coe, H., Allen, G., Vaughan, G., Daum, P., Fairall, C., Chand, D., Gallardo Klenner, L., Garreaud, R., Grados Quispe, C., Covert, D. S., Bates, T. S., Krejci, R., Russell, L. M., de Szoeke, S., Brewer, A., Yuter, S. E., Springston, S. R., Chaigneau, A., Toniazzo, T., Minnis,

P., Palikonda, R., Abel, S. J., Brown, W. O. J., Williams, S., Fochesatto, J., and Brioude, J.: The VAMOS Ocean-Cloud-Atmosphere-Land Study Regional Experiment (VOCALS-REx): goals, platforms, and field operations, Atmos. Chem. Phys. Discuss., 10, 20769–20822, doi:10.5194/acpd-10-20769-2010, 2010. 686, 688, 695, 697

Wyant, M. C., Wood, R., Bretherton, C. S., Mechoso, C. R., Bacmeister, J., Balmaseda, M. A., Barrett, B., Codron, F., Earnshaw, P., Fast, J., Hannay, C., Kaiser, J. W., Kitagawa, H., Klein, S. A., Köhler, M., Manganello, J., Pan, H.-L., Sun, F., Wang, S., and Wang, Y.: The PreVOCA experiment: modeling the lower troposphere in the Southeast Pacific, Atmos. Chem. Phys., 10, 4757–4774, doi:10.5194/acp-10-4757-2010, 2010 685

Zhang, Q., Jimenez, J. L., Worsnop, D. R., and Canagaratna, M. R.: A case study of urban particle acidity and its effect on secondary organic aerosol, Environ. Sci. Technol., 41(9), 3213–3219, doi:10.1021/es061812j, 2007. 709

Zhang, S. H., Akutsu, Y., Russell, L. M., Flagan, R. C., and Seinfeld, J. H.: Radial differential mobility analyzer, Aerosol. Sci. Tech., 23, 357–371, 1995. 692, 729

Zorn, S. R., Drewnick, F., Schott, M., Hoffmann, T., and Borrmann, S.: Characterization of the South Atlantic marine boundary layer aerosol using an aerodyne aerosol mass spectrometer, Atmos. Chem. Phys., 8, 4711–4728, doi:10.5194/acp-8-4711-2008, 2008. 708

Table 1. Flight designators for data used in this study. Flights with the prefix "B" define those by the BAe-146, "RF" corresponds to the NSF-C130 and "G" to the DoE-G1 aircraft.

Platform	Flights
BAe-146	B409,B410,B411,B412,B414,B417,B419,B420
DoE-G1	G081014,G081017,G081018,G081022,G081023,G081025,G081026,G081027, G081028,G081029,G081101,G081103,G081104,G081106,G081108, G081109,G081110,G081112,G081113
NSF-C130	RF01,RF02,RF03,RF04,RF05,RF06,RF07,RF08,RF09,RF10,RF11,RF12,RF13,RF14

Table 2. Selected aerosol and trace gas instruments onboard the various platforms considered in this study. Measured particle size ranges (as sampled particle diameter) are stated where appropriate.

Platform	Instrument	Aerosol size/gas	Technique	Ref/Company
BAe-146	PCASP	0.1–3.0 µm	Optical scattering	PMS Inc
	SMPS	15–600 nm	Differential mobility	Wang et al. (1990)
	VACC	0.1–0.5µm	Volatility	Brooks et al. (2002)
	AMS	0.04–0.7 µm	ToF mass spectrometry	Jayne et al. (2000)
	CO	Carbon monoxide	UV Fluorescence	Aerolaser Inc AL5002
	O_3	Ozone	UV absorption	2B Technologies
	CPC	Total (0.01–3.0 µm)	Condensation	TSI Inc Model 3010
DoE-G1	PCASP	0.1–3.0 µm	Optical scattering	PMS Inc
	SMPS	15–600 nm	Differential mobility	Wang et al. (1990)
	CO	Carbon monoxide	UV fluorescence	Resonance Ltd
	O_3	Ozone	UV absorption	Thermo Electron Model 49–100
	SO_2	Sulphur dioxide	Pulsed fluorescence	Thermo Electron Model 43S
	AMS	0.04–0.7 µm	Quadrupole mass spectrometry	Jayne et al. (2000)
NSF-C130	O_3		UV absorption	Thermo Electron Model 49–100
	SO_2	Sulphur dioxide	APIMS	Drexel Univ.
	O_3	Ozone	UV Absorption	TECO 49 UV
	CO	Carbon monoxide	UV Fluorescence	NCAR
	SMPS	10–150 nm	Differential mobility	Zhang et al. (1995)
	LAS-X	0.15–10.0 µm	Optical scattering	PMS Inc
	AMS	0.04–0.7 µm	ToF mass spectrometry	De Carlo et al. (2006)
	CPC3010	Total (0.01–3.0 µm)	Condensation	TSI Inc Model 3010
	CPC3025	Total (0.025–3.0 µm)	Condensation	TSI Inc Model 3025
RHB	AMS	0.04–0.7 µm	Quadrupole mass spectrometry	Bates et al. (2008)
Paranal/Paposo	DMPS	10–400 nm	Differential mobility	Stockholm Univ.
	Grimm	0.26–2.2 µm	Optical scattering	Grimm Inc Model 3.709

Table 3. VACC zonal mean particle number concentration for the identified chemical compounds. Concentrations are expressed as percentage of the integrated number concentration in the diameter range 0.1–0.5 µm.

Zones	Org	VOC	AHS	MSA	AN	AS	Core
Coast	5.9	4.3	0.0	17.5	5.9	58.5	6.3
Transition	5.3	3.0	2.9	17.4	9.4	47.9	8.3
Remote	9.3	7.7	0.0	20.1	10.2	41.4	7.9

Table 4. Lognormal fit parameters to campaign-mean aerosol size spectra in each longitude zone below 1200 m (MBL) and between 1700 m and 3200 m (FT). Errors quoted represent a one standard deviation uncertainty on the fitted parameter. All quantities are accurate to 3 d.p.

Mode	Param	0 m<altitude<1200 m (MBL)			1700 m<altitude<3200 m (FT)		
		Coast	Trans	Remote	Coast	Trans	Remote
1	N_{tot}	20.065±0.009	13.278±0.803	46.642±1.730	32.804±3.871	113.554±4.878	n/a
	$\ln\sigma_g$	0.435±0.000	0.260±0.019	0.348±0.015	0.188±0.026	0.217±0.011	n/a
	D_g	0.014±4.740	0.013±0.000	0.018±0.000	0.014±0.000	0.013±0.000	n/a
2	N_{tot}	114.996±0.007	155.108±1.085	153.421±1.737	0.381±5.264	87.790±6.294	n/a
	$\ln\sigma_g$	0.353±2.790	0.497±0.004	0.354±0.004	0.344±5.390	0.369±0.030	n/a
	D_g	0.050±1.710	0.042±0.000	0.039±0.000	0.036±0.246	0.036±0.001	n/a
3	N_{tot}	268.099±0.008	175.766±1.017	166.774±1.992	368.097±6.643	53.875±8.202	n/a
	$\ln\sigma_g$	0.444±1.704	0.429±0.002	0.465±0.006	0.556±0.011	0.621±0.113	n/a
	D_g	0.157±3.272	0.158±0.000	0.154±0.001	0.076±0.001	0.147±0.020	n/a
4	N_{tot}	15.347±0.012	0.813±1.724	n/a	5.851±4.324	n/a	n/a
	$\ln\sigma_g$	0.310±0.000	0.350±0.860	n/a	0.069±0.052	n/a	n/a
	D_g	0.619±0.000	1.839±1.808	n/a	0.631±0.060	n/a	n/a

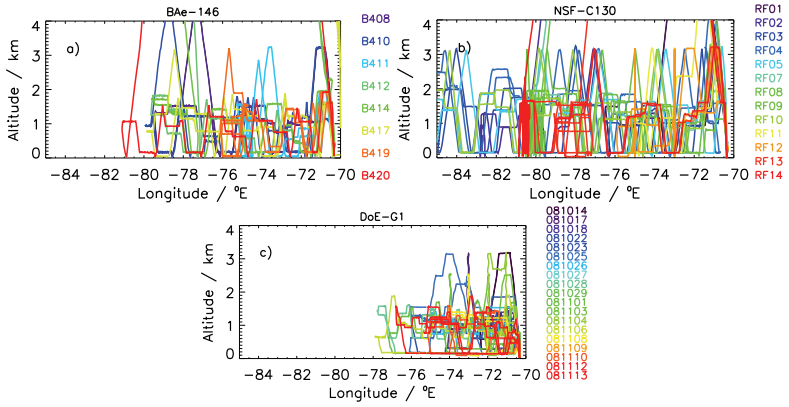

Fig. 1. Flight tracks as longitude-altitude cross-sections of VOCALS-REx flights used in this study and within 1-degree latitude of the 20° South parallel. Individual flight tracks are colour-coded to individual flights to illustrate sampling throughout the course of the VOCALS campaign. Each panel illustrates flight tracks from each of the aircraft platforms as labelled.

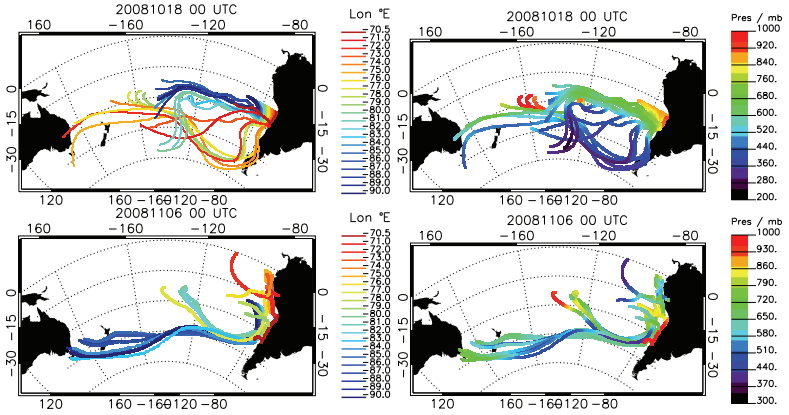

Fig. 2. Ten-day free tropospheric backward airmass trajectories ending at 850 hPa along 20° S initiated at 0.5 degree intervals between 70.5° W and 90° W at 00:00 UTC on 18 October 2008 (top) and 6 November 2008 (bottom). Left panels are colour-coded for longitudinal end-point, whilst right panels are colour-coded for pressure along each trajectory.

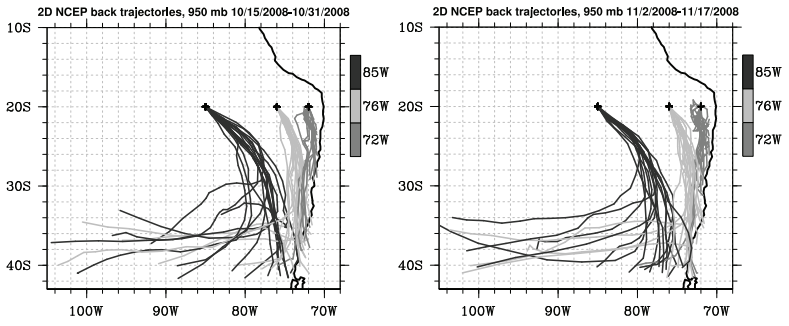

Fig. 3. Five-day isobaric (950 hPa) boundary layer airmass backward trajectories initiated at 72° W, 76° W and 85° W as grey-scaled, initiated daily at 00:00 UTC throughout 15–31 October and 1–15 November, respectively. Trajectories terminate on surface contact.

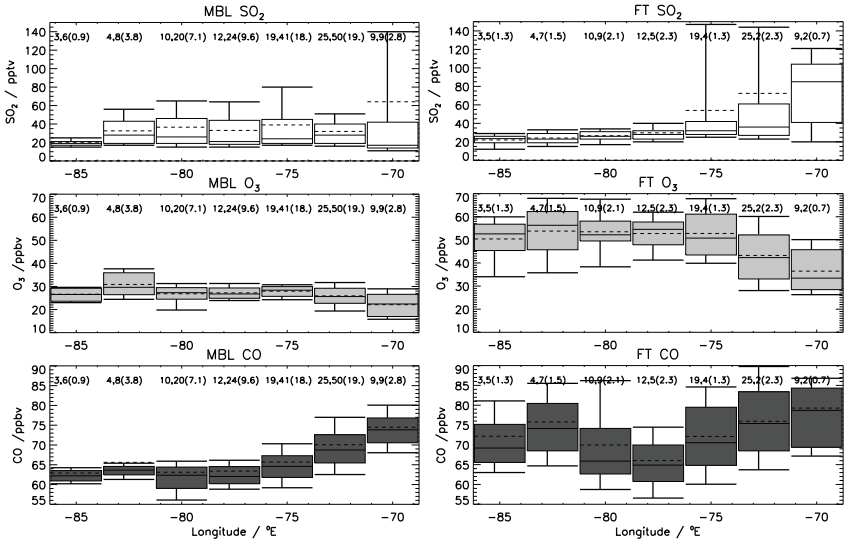

Fig. 4. Sulphur dioxide (top panels), ozone (centre panels) and carbon monoxide (lower panels) concentration statistics in the MBL (left panels) and the FT (right panels) gridded into 2.5 degree longitudinal zones along the 20° South parallel averaged from aircraft measurements during VOCALS-REx. For each zone, thick centre lines indicate the median, dashed lines indicate the mean, boxes indicate upper and lower quartiles with upper and lower decile whiskers. Plotted above each longitude zone and for each panel, numbers before the comma indicate number of flights contributing to each statistic, followed by the number of straight and level runs, with the total sampling time in decimal hours in parentheses.

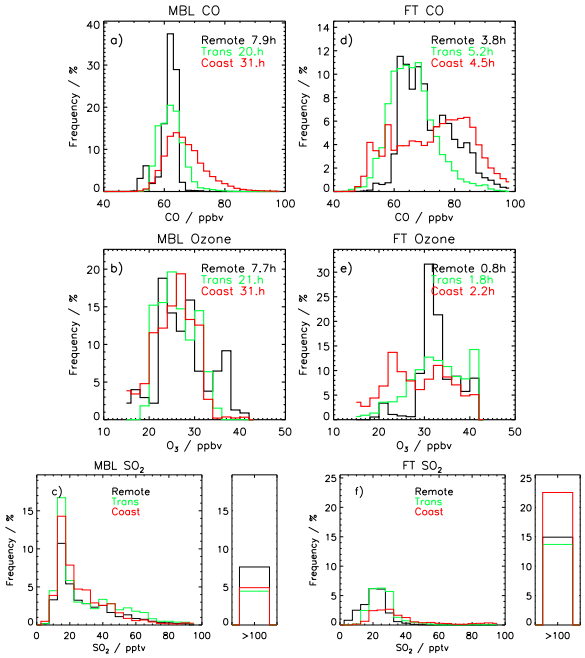

Fig. 5. All-aircraft carbon monoxide (top panels), ozone (centre panels) and sulphur dioxide (lower panels) concentration probability density functions gridded into longitudinal zones (colour-coded as indicated) along 20° S, in the MBL (left panels) and the FT (right panels). Total sampling time in hours is plotted in each panel for each zone. See text for further details.

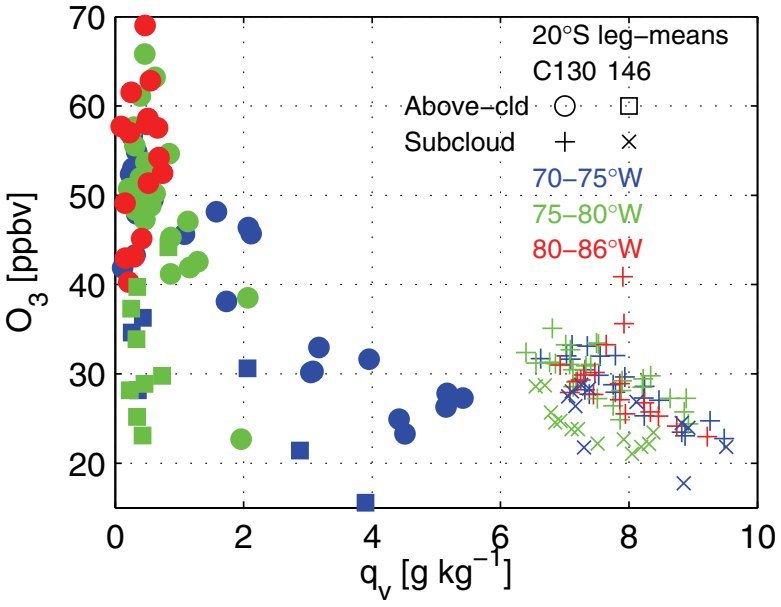

Fig. 6. Scatter plot of ozone concentration versus specific humidity from aircraft measurement, colour-coded for longitudinal zones and symbolized for aircraft platform and location below or above cloud, as detailed in the figure legend.

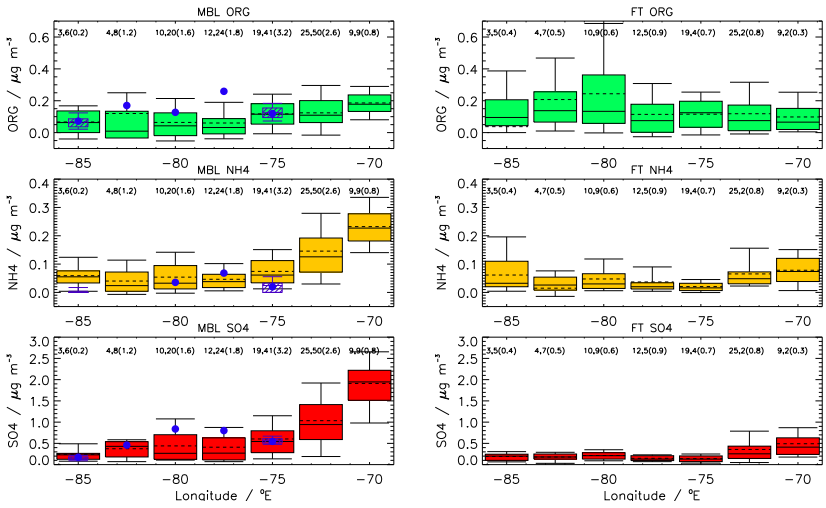

Fig. 7. Longitudinally-gridded aerosol mass concentrations for: organics (green, top panels); ammonium (yellow, middle panels); and sulphate (red, bottom panels) for the marine boundary layer between 10–1200 m (left panels) and the free troposphere between 1700–3200 m (right panels). For each zone, thick centre lines indicates the sample median, dashed lines indicates the mean, boxes indicate upper and lower quartiles with upper and lower decile whiskers. Median mass concentrations measured by the Ron Brown research vessel are plotted as purple circles for the marine boundary layer, with purple box and whisker plots for periods when the Ron Brown was anchored on station. Plotted above each longitude zone and for each panel, numbers before the comma indicate number of flights contributing to each statistic, followed by the number of straight and level runs, with the total sampling time in decimal hours in parentheses.

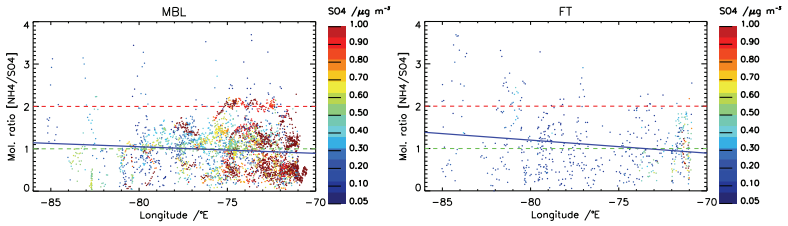

Fig. 8. Ammonium to sulphate molar mass ratio plotted as a function of longitude below 1200 m altitude (left panel) and between 1700 m and 3200 m (right panel). A dashed green line defines a molar ratio of unity and red a ratio of 2.

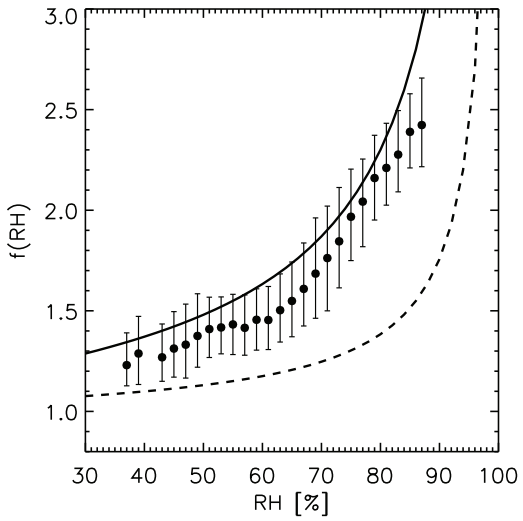

Fig. 9. Composite humidogram of wet nephelometer data recorded in the MBL. Filled circles are the median and the error bars the upper and lower quartiles of 1 Hz data gridded in 2% RH bins.

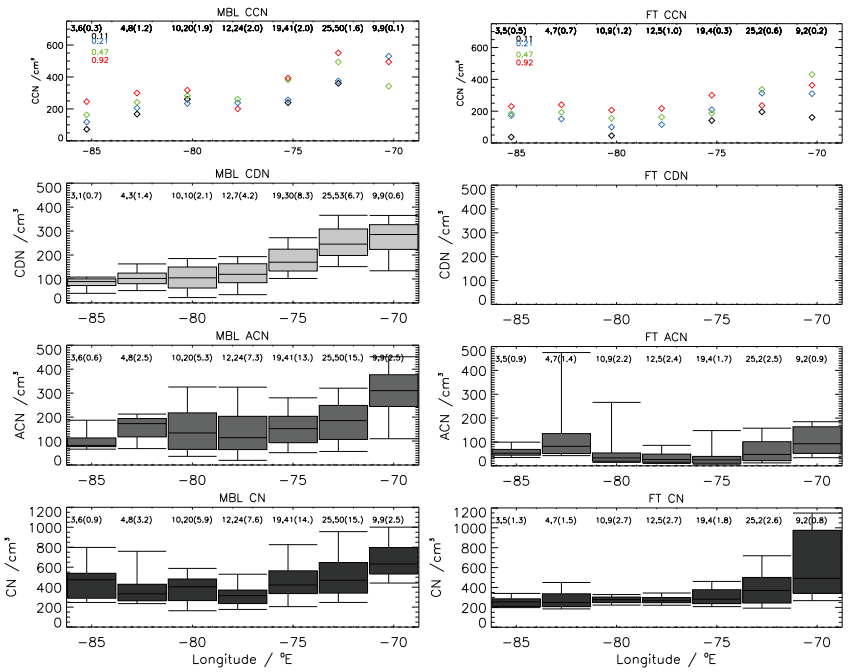

Fig. 10. Aerosol concentration and cloud physics measurement statistics averaged into 2.5-degree longitude zones below 1200 m altitude (left panels) and between 1700–3200 m altitude (right panels). For each vertical domain, cloud condensation nucleus concentration (CCN), cloud droplet number (CDN), accumulation mode aerosol concentration (ACN) and total condensation nuclei greater than 10 nm particle diameter (CN) are plotted as titled. With the exception of CCN data, for each longitude zone, thick centre lines indicates the sample median, dashed lines indicate the mean, boxes indicate upper and lower quartiles with upper and lower decile whiskers. Only median data are presented for CCN, colour-coded to supersaturation as labeled in the figure. Plotted above each longitude zone and for each panel, numbers before the comma indicate number of flights contributing to each statistic, followed by the number of straight and level runs, with the total sampling time in decimal hours in parentheses.

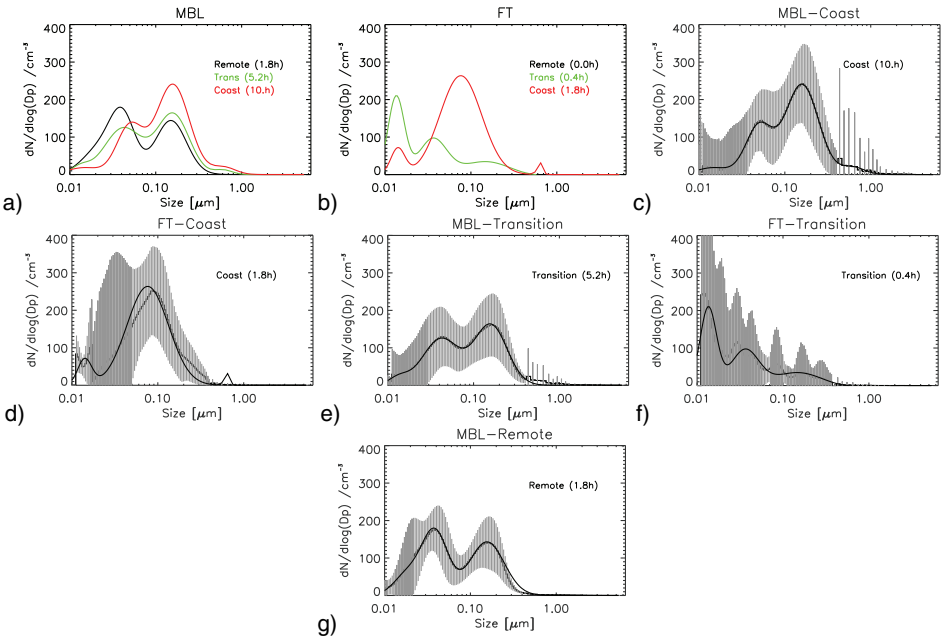

Fig. 11. Particle number size distributions (normalised to natural logarithm of bin width) and log-normal fitted functions between 10 nm and 5 µm in the MBL and FT as labeled, with total sampling time in hours in parentheses: **(a)** Log-normal fitted functions to median aerosol number spectra for each longitude zone labeled as coloured; **(b)** Median MBL coastal zone spectrum (stepped grey line) with corresponding log-normal fit (solid black line); **(c)** Transition zone MBL spectrum; **(d)** Remote zone MBL spectrum; **(e)** Log-normal fitted functions for each longitude zone labeled as coloured for the free troposphere; **(f)** Coastal zone FT spectrum; **(g)** Transition zone FT spectrum. Note: A remote zone FT spectrum was not sampled. For each sizing channel, grey bars illustrate one-standard-deviation of the measurement around the median in each channel. Stepped black lines define the median concentration in each sizing channel, whilst the smooth solid black line illustrates the corresponding log-normal fit.

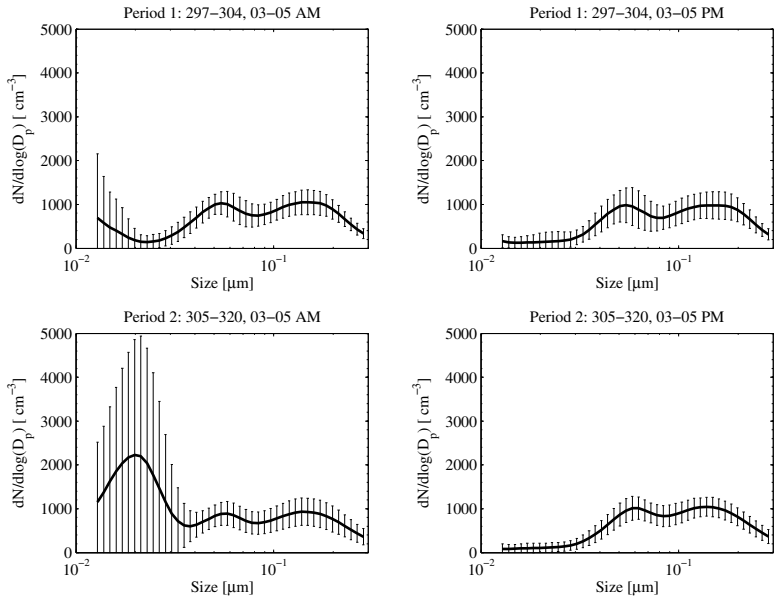

Fig. 12. Mean aerosol number size distributions (normalized for bin width to base-10 logarithm) between 0.01 and 0.3 µm diameter with one-standard-deviationbars as measured at Paposo (690 m a.m.s.l.). Upper panels show data recorded between 15 and 30 October 2008 (Period 1) and lower panels are for the period 1 to 15 November 2008 (Period 2), between 3–5 a.m. local time (left panels) and 3–5 p.m. local time (right panels). The day-of-year range is given in the title for each panel.

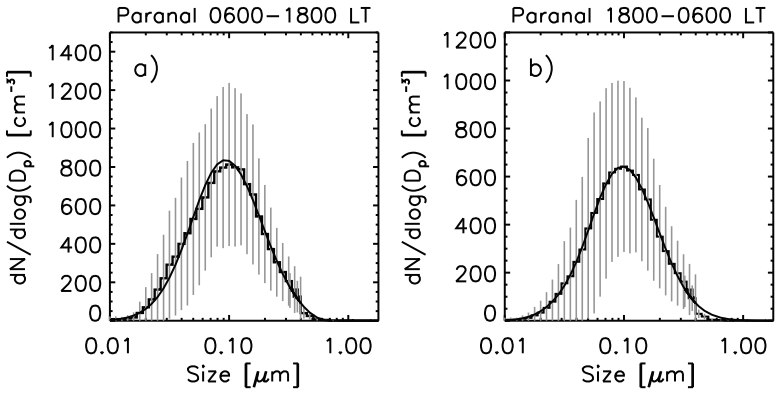

Fig. 13. Mean aerosol number size distributions (normalized for bin width to base-10 logarithm) between 0.01 and 1.1 µm diameter with one-standard-deviation bars as measured at Paranal (2635 m a.m.s.l.) between **(a)** 18:00 and 06:00 LT (left panel); and **(b)** 06:00 and 18:00 LT (right panel).